Solar Radio Spectro-polarimeter (50-500 MHz). I. Design, Development, and Characterization of a Cross-polarized, Log-periodic Dipole Antenna

(article starts on next page)

CrossMark

Solar Radio Spectro-polarimeter (50–500 MHz). I. Design, Development, and Characterization of a Cross-polarized, Log-periodic Dipole Antenna

Anshu Kumari[1,5] ⓘ, G. V. S. Gireesh[2], C. Kathiravan[2] ⓘ, V. Mugundhan[3,5], Indrajit V. Barve[2], R. Ramesh[2] ⓘ, and C. Monstein[4]
[1] NASA Postdoctoral Program Fellow, NASA Goddard Space Flight Center, Greenbelt, MD 20771, USA
[2] Indian Institute of Astrophysics, II Block, Koramangala, Bangalore 560034, India; kathir@iiap.res.in
[3] Department of Earth and Space Sciences, Chalmers University of Technology, Onsala Space Observatory, SE-439 92 Onsala, Sweden
[4] Istituto ricerche solari Aldo e Cele Daccò (IRSOL), Università della Svizzera italiana (USI), CH-6605 Locarno, Switzerland

Abstract

The Zeeman effect has been routinely used to image and quantify the solar photospheric magnetic field (B). Such a direct measuring technique is not yet available for the corona (Lin et al. 2004). Since almost all transient nonthermal radio emissions from the corona are either partially or fully circularly polarized, observing their polarization signatures over broad frequency ranges would be of help to estimate B as a function of heliocentric height. This article aims to describe the design and development of a Cross-polarized Log-Periodic Dipole Antenna (CLPDA), an integral part of a radio spectro-polarimeter, which works in the 50–500 MHz frequency-range and to explain the tests that were carried out to characterize it. The above frequency range corresponds to a heliocentric height range $\approx 1.03 < r < 2.5\,R_\odot$ ($R_\odot = photospheric\ radius$), wherein the numerous coronal nonthermal transients associated with space-weather effects are observed to originate. The CLPDA is used to determine the strength and sense of polarization of the received radio signal. The uncertainty involved in the determination depends on the polarization-isolation (PI) between the two orthogonal components of a CLPDA. Some of the recent advancements made in the antenna design concepts at high frequencies ($\sim$GHz) were adopted to reduce the PI at low frequencies ($\sim$MHz). Throughout the above frequency range, the CLPDA has a gain, return loss, and PI of ≈ 6.6 dBi, $\lesssim -10$ dB, and $\lesssim -27$ dB, respectively. The average PI of the CLPDA varies from -30 to -24 dB over an azimuthal angle range $0°$ to $\pm 45°$ within which the observations are performed regularly.

1. Introduction

The performance of space-based technological systems depends on the weather conditions (called space weather[6]) that prevail in the Earth's geospace. Space weather (SW) can be disastrous (Lanzerotti 2004; Gary 2008) at times due to transient activities such as flares and coronal mass ejections (Schwenn 2006) that take place in the outer solar atmosphere. Identifying the precursors of such events would therefore become essential to forecast SW reliably in order to safeguard space-based systems. In the latter context, different types of radio bursts (type-III, V, etc.) were recognized to be some of the precursors (Cane 2002; Aschwanden 2006) of above transients, especially in the low-frequency radio regime. Observational studies show that the onset of the aforementioned radio bursts is predominantly decided by the strength, configuration, and spatio-temporal evolution of the associated solar active-region and ambient magnetic field (B) system (Allen 1947; Gopalswamy & Kundu 1987; Reid & Ratcliffe 2014). Furthermore, the changes in B near the source region of the above transients are essential ingredients to understand the strength and nature of the associated energy release (Ramesh et al. 2020) and the

polarization state as well. While the radio emission mechanism may be different (McLean 1985; Carley et al. 2020) in different frequency ranges, the measured circular polarization always contains some information about B of the source region (refer Ramesh et al. 2010; Hariharan et al. 2015; Kumari et al. 2019; Alissandrakis & Gary 2021; Ramesh & Kathiravan 2022, and the references therein). One may generally ignore linear polarization of the radio emission, particularly at low frequencies, since Faraday rotation of the plane of linear polarization is so large and frequency dependent that it is washed out when the radio emission is summed over any normal observing bandwidth (Hatanaka 1956; Grognard & McLean 1973). Therefore, one may utilize the circular polarization signatures, obtained through high time and frequency resolution observations, to improve the SW forecasts and to study the various aspects of transients (Morosan et al. 2022), in general. Since the aforementioned transient events were found to originate in the low and middle corona (from where radio waves of 50–500 MHz emanate), commissioning a broadband solar radio spectro-polarimeter (SP) that can observe the corresponding portion of coronal region would be productive. The new SP setup at our observing time zone (03:00–09:00 UT) would overlap with the existing ones and can fill the temporal observational gap. Also, it would be a useful addition since the number of solar SP that are being operated routinely around the globe in the above frequency band is smaller as compared to the number of spectrographs. Moreover, as pointed out by Dumas et al. (1982), any new addition to a suite of existing dedicated observing facilities at

---

an observatory would benefit the research community both on scientific and technical grounds. The present work is motivated by the scientific and technical accomplishments of various research groups that built and commissioned several solar radio spectrometer and SP instruments in the past across the globe. One may refer to the articles listed here and the references therein to know those groups and their technical contributions: Wild & McCready (1950), Wild et al. (1954), Thompson (1961), Mosier & Fainberg (1975), Kaverin et al. (1979), Dumas et al. (1982), Perrenoud (1982), Jin et al. (1986), Allaart et al. (1990), Benz et al. (1990), Mann et al. (1992), Bogod et al. (1993), Jiricka et al. (1993), Prestage (1995), Sawant et al. (2001), Fu et al. (2004), Kontogeorgos et al. (2006), Ebenezer et al. (2007), Benz et al. (2009a, 2009b), Zucca et al. (2012), Antar et al. (2014), Kishore et al. (2014), Kishore et al. (2015), Du et al. (2017), Puricer et al. (2019), and Hamini et al. (2021). In addition to the above, the recently built large radio facilities such as the Long Wavelength Array (Ellingson et al. 2009), the Murchison Widefield Array (Tingay et al. 2013), and the LOw-Frequency ARray (Van Haarlem et al. 2013) have been used to observe the low-frequency radio spectral and spectro-polari-metric signatures of the Sun with high spatial, temporal, and frequency resolution, through proposals. At this juncture, it has to be noted here that many of the major inputs accountable for the current understanding of the SW and solar radio astronomy in general, came from the observations obtained with instruments built since 1950.

A radio SP consists of three major subsystems: the analog frontend, the digital backend, and the data acquisition system. The principal component of a frontend receiver is a radio antenna. One of the wideband-antenna types that has been recently used is a Cross-polarized Log-Periodic Dipole Antenna (CLPDA; refer to Section 2 for details; Wu 1969; Van Nieuwkoop 1971; Dumas et al. 1982; De Lera Acedo et al. 2015). The CLPDA helps us to determine the strength and sense of polarization of a received signal. The accuracy of the determination is dependent on the polarization-isolation (PI; refer to Section 3.2 for details) that a CLPDA can offer (De Lera Acedo et al. 2015). Through novel simulations and prototype designs using miniature printed circuit board (PCB)–based high-frequency Log-Periodic Dipole Antennas (LPDAs; refer to Section 2 for details, and Keen 1974, Campbell et al. 1977, and Pantoja et al. 1987 for the early PCB-microstrip-based LPDA designs), Pivnenko (2006) demonstrated that the PI can be reduced to values below that of the conventional design. So, we explored the possibility of utilizing the same design concept for a CLPDA that can work in the low-frequency regime with a low PI; additionally, we intended to reduce, as much as possible, the dimensions of the CLPDA with respect to its conventional design in order to minimize the fabrication and installation complexities, costs, efforts, etc., without compromising its reception characteristics. As far as the miniaturization of an LPDA is concerned, techniques such as Koch fractalization (Puente-Baliadra & Pous 1996; Strycek & Hertl 2007; Anagnostou et al. 2008), meandering (Rashed & Tai 1991; Best 2002; Geethan & Anagnostou 2008; Lee et al. 2010), meta-material (Greiser 1964; Breed 2008; Ripin et al. 2013; Zhai et al. 2019), top-loading (DiFonzo 1964; Simpson 1971; Gong et al. 2012; Kyei et al. 2017), the hybrid (Genetic Algorithm and Nelder-Mead simplex) optimization (Chung & Haupt 2001; El-Khamy et al. 2004), and dual-band dipoles (Kyei & Jung 2018) are being used to design LPDAs

for high-frequency communication applications. The fractaliza-tion method reduces the transverse dimensions of an LPDA by ≈10%–17%; however, its directivity may vary by a factor of 2 or higher (Qiu et al. 2005; Moallemizadeh et al. 2012), and its operating bandwidth may also be reduced (Anagnostou et al. 2008; Jingjing et al. 2008). Furthermore, we note that the higher-order fractalization on antenna miniaturization is less significant; the PI will also be lowered as compared to the corresponding conventional design, due to miniaturization. Though the meandering technique reduces the size of an antenna drastically, the direction of maximum transmission or reception changes from one frequency to another within the operating bandwidth (Jamil et al. 2011). This will introduce additional complexities in the calibration at later stages. One of the shortcomings of a meta-material type is its significantly radiating ground plane; Breed (2008) indicated that modeling the latter is difficult due to large uncertainties involved. Also, the design has a limitation in terms of side and back lobes that reduces the antenna gain (Ripin et al. 2013). The top-loading technique also works well in reducing the transverse dimension of the LPDA up to ≈26%–60%; yet, the gain of the antenna is found to vary excessively in addition to the shape-changes in the radiation patterns as a function of frequency (Rahman & Jamlos 2016); moreover, a split in the front lobe of the LPDA is observed at high frequencies (Gong et al. 2012) along with higher back-lobe levels at low frequencies (Sun et al. 2014). El-Khamy et al. (2004) showed that the hybrid optimization (GA +N-M Simplex) can reduce the length and the number of dipoles of an LPDA to half of its conventional design. However, the algorithm seems to work well for narrow bands (∼2:1), and for broadbands (∼5:1), higher variation in gain and VSWR can be noticed. Pitzer et al. (2006) noted that the GA results are not promising, as the side lobes are not minimized at a few angles. Additionally, the GA does not seem to be robust in searching the parameter-space of LPDA, although good VSWR profiles are achieved; the inclusion of side and back-lobe level requirement in GA has not facilitated the improve-ments as expected. The dual-band technique also reduces the length of the antenna by ∼40% with good reflection loss profile. Still, the gain is found to vary drastically and is also lesser than the conventional design. From many of the publications cited above, it can be inferred that the size reduction has been carried out extensively only along the transverse dimension. Note that only a few have focused on the reduction along the axial dimension (RAD), i.e., along the transmission line of an LPDA (Bantin & Balmain 1970; Kyei & Jung 2018). Though Bantin & Balmain (1970) concluded that the size reduction along the transmission line retains frequency independence, a larger reduction ($\alpha \gtrsim 40°$; α is the half-apex angle of the LPDA; refer to Section 2.1 for the definition) leads to rise in back-lobe level, lowering of input resistance and gain, increase in VSWR, and a marked sensitivity to mechanical vibration. Thus, it is evident from the above discussion that the true dimension reduction of an LPDA would be at the cost of efficiency (Jones & Mayes 1969), bandwidth deterioration/reduction, pattern distortion (Rashed & Tai 1991), and so on. Therefore, we decided to go for a reasonable RAD by following a procedure closer to the conventional approach to circumvent the problems due to miniaturization mentioned above. A reasonable RAD (i.e., designs having $\alpha \lesssim 40°$) is expected to overcome the structural instabilities that could arise due to slight mechanical vibrations
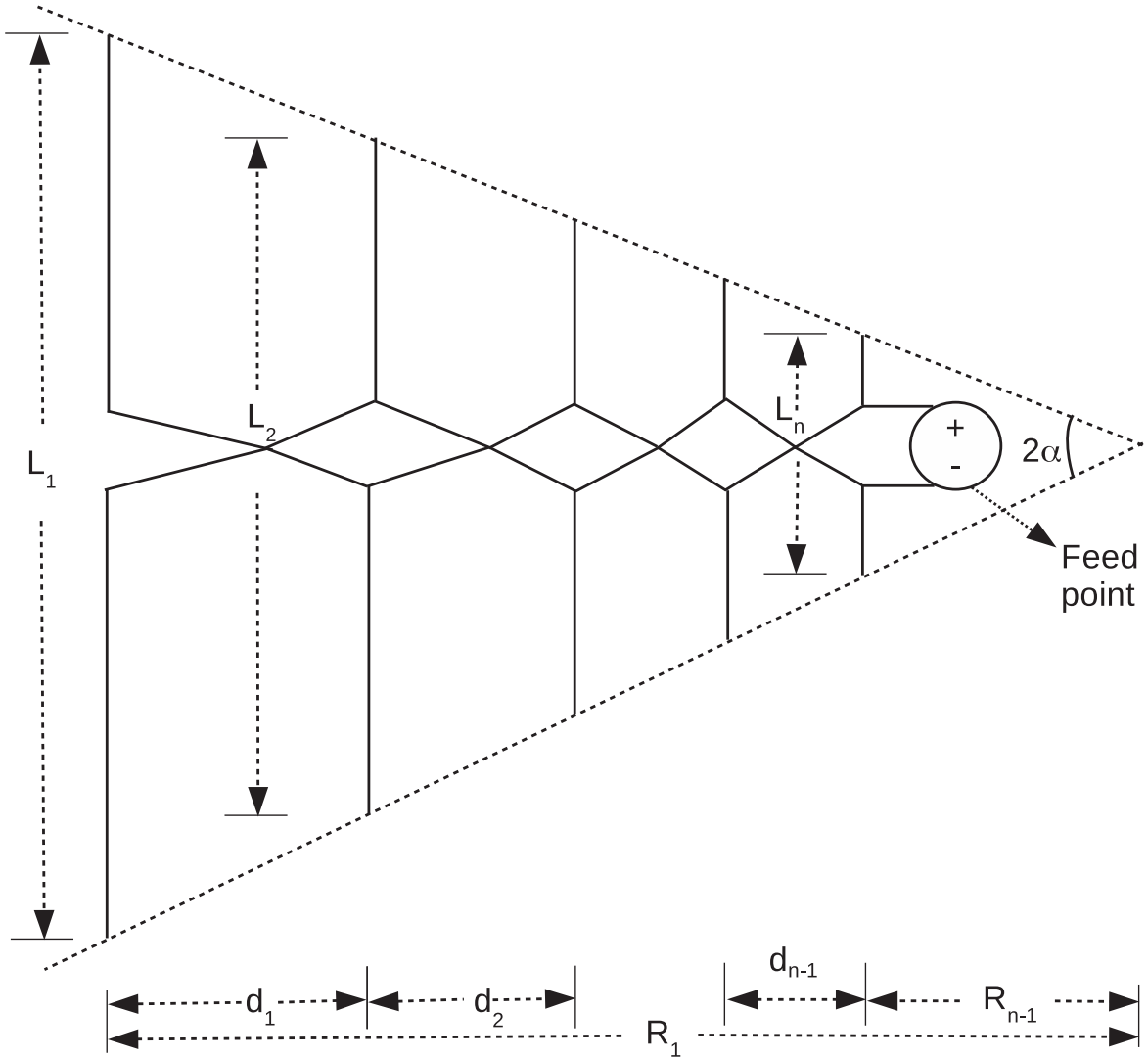
Figure 1. Schematic diagram of an LPDA (not to scale).

leading to oscillatory impedance fluctuations (Bantin & Balmain 1970). In the conventional approach, the higher-frequency cutoff is a free parameter. But, in our approach, it is roughly a fixed value, and the spacing factor (σ; refer to Section 2.1 for the definition of σ) is allowed to vary semi-freely around the conventional value by slightly increasing the number of dipoles from the conventional design, within the operating bandwidth. This allows us to retain the conventional LPDA characteristics, as can be inferred from the following discussions. As a result, we developed a new moderately sized aluminum extrusion based broadband CLPDA prototype that can work in the 50–500 MHz band (operating bandwidth "OB", henceforth) with approximately constant gain, good VSWR, and reasonably high PI, throughout the OB. Further, from the following discussions, it can passably be concluded that small changes to the parametric values of the initial conventional LPDA design would : (i) bring the impedance of the LPDA/CLPDA closer to the characteristic value ($50\,\Omega$) throughout the OB; (ii) help achieving a constant directional gain throughout the OB; (iii) reduce its size as compared to the conventional optimum design; and (iv) make it an impedance-transformer-free antenna, which might be unavoidable for higher RAD (Bantin & Balmain 1970).

The present article (Part I of the Solar Radio Spectro-polarimeter (50–500 MHz)) is prepared to cover in detail the design, development, and characterization of a broadband CLPDA, the frontend of the SP, constructed at the Gauribida-nur Observatory (Ramesh et al. 1998; Ramesh 2011). The technical details are elaborated in Sections 2 and 3. Section 2 explains the development of the LPDA, its design constraints, impedance, and the procedure adopted to fine-tune it. Section 3 discusses the construction of CLPDA using the prototype LPDA, the measurements of field patterns, and PI of the CLPDA. Section 4 discusses the conclusions and future prospects. The subsequent article (Part II of the Solar Radio Spectro-polarimeter (50–500 MHz)) will describe in detail the digital backend receiver, the data acquisition system, and its validation through observations, with the new CLPDA described here as the frontend module.

2. Design and Development of CLPDA

A CLPDA is a combination of two identical LPDAs; both LPDAs share a common vertical axis; however, the orientation of dipoles of one of the antennas is orthogonal to the other (De Groot & Van Nieuwkoop 1968; Wu 1969; Dumas et al. 1982; Wakabayashi et al. 1999; Sasikumar raja et al. 2013;
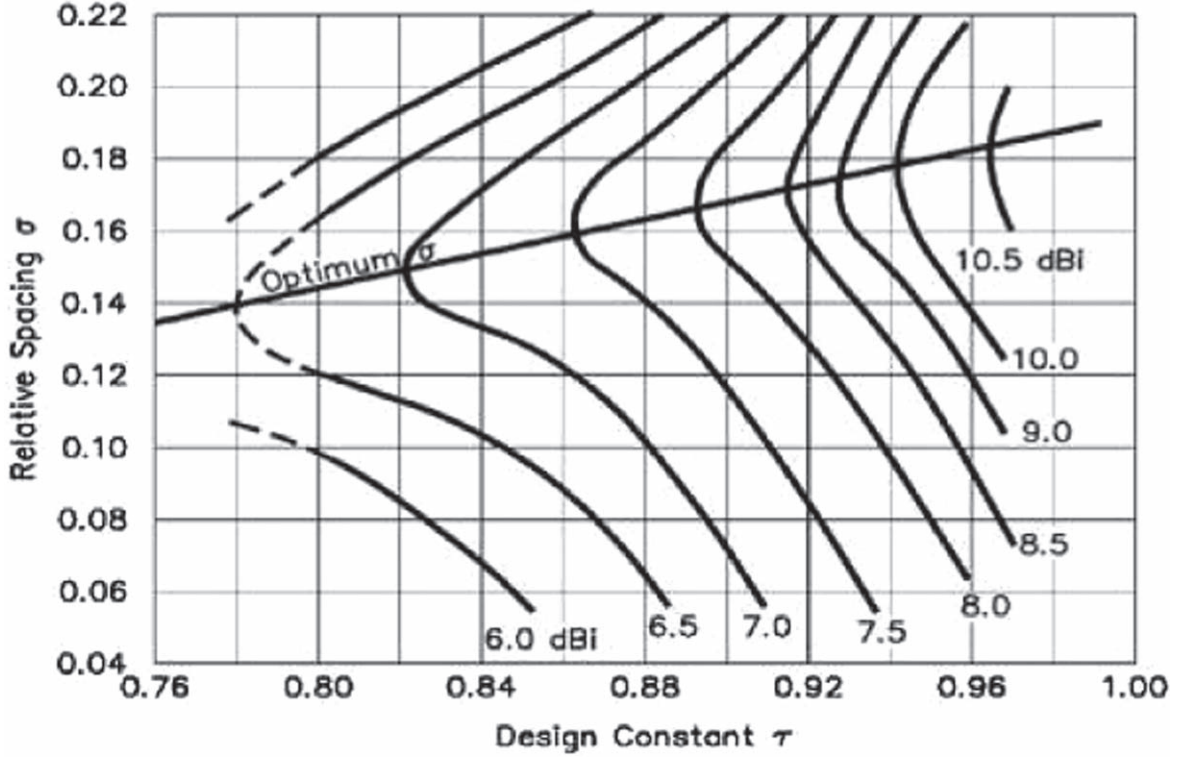
Figure 2. Plot of LPDA directional gain as a function of design parameters τ and σ (reproduced from Carrel 1961a).

Table 1
LPDA: Initial Design Specification (50–500 MHz)

S. No.	D	S	L	F
	(cm)	(cm)	(cm)	(MHz)
(1)	(2)	(3)	(4)	(5)
1.	0.0	0.0	13.5	555.6
2.	4.0	4.0	15.5	483.9
3.	9.0	5.0	18.0	416.7
4.	15.0	6.0	21.0	357.1
5.	22.0	7.0	24.5	306.1
6.	30.0	8.0	28.5	263.2
7.	39.0	9.0	33.0	227.3
8.	50.0	11.0	38.5	194.8
9.	63.0	13.0	45.0	166.7
10.	77.0	14.0	52.0	144.2
11.	94.0	17.0	60.5	124.0
12.	114.0	20.0	70.5	106.4
13.	137.0	23.0	82.0	91.5
14.	164.0	27.0	95.5	78.5
15.	195.0	31.0	111.0	67.6
16.	231.0	36.0	129.0	58.1
17.	273.0	42.0	150.0	50.0

Note. Column (2): distance from the apex; column (3): half-dipole length ($\lambda/4$); column (4): frequency ($F = c/\lambda$); column (5): diameter of the dipoles.

Bolli et al. 2020). The vertical axis is a fictitious equi-divider line drawn in between the transmission lines of an LPDA. Obviously, to construct a CLPDA, two identical LPDAs are required at hand a priori.

2.1. Introduction to LPDA

By definition, an LPDA is a coplanar array of dipoles (Isbell 1960); it has unequal length and unequally spaced

parallel and linear dipoles (Cheong & King 1967) that are fed alternatively (180° phase difference between adjacent dipoles) by a parallel transmission line with a desired characteristic impedance. The electrical characteristics of it vary periodically with the logarithm of frequency (Isbell 1960; DuHamel & Isbell 1966), hence the name "LPDA"; refer Figure 1 for the schematic. Empirical relationships suggested by Carrel (1961a) are usually followed to design an LPDA. The lowest and highest operating-frequencies, f_1 and f_n, respectively, are related to each other such that $f_1 = \tau^{n-1} f_n$, where τ is the geometric constant, one of the design parameters. The relationship between length of adjacent dipole arms (L_n and L_{n-1}), the spacing between them (d_n), and their distances from the apex (R_n and R_{n-1}), respectively, of an LPDA is given in Equation (1).

$$\tau = \frac{L_n}{L_{n-1}} = \frac{R_n}{R_{n-1}} = \frac{d_{n-1}}{d_{n-2}}. \tag{1}$$

The other two design parameters are the spacing factor (σ) and the half-apex angle (α). The parameter σ is defined as the ratio of the distance between adjacent elements to twice the length of the larger element, and the parameter α is defined as the angle subtended by an imaginary line passing through the one end of the dipoles with respect to the center line of the antenna (Carrel 1961b). By fixing any two design parameters, the third one can be determined using Equation (2).

$$\sigma = \frac{1-\tau}{4\tan\alpha}. \tag{2}$$

The relationship between the geometric constant, half-apex angle and inter-dipole spacing factor of an LPDA is given in Equation (2). The length of the longest dipole is equal to half of the maximum wavelength (λ_{max}) of operation.
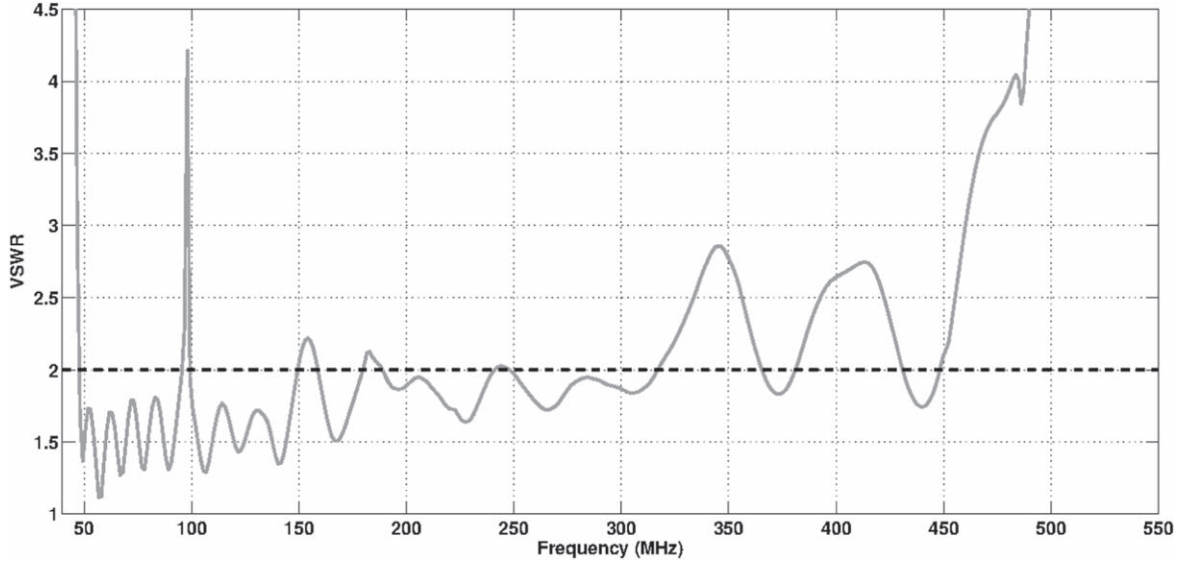
Figure 3. VSWR of the prototype LPDA as a function of frequency; the horizontal line drawn at VSWR equal to 2.0 shows a power transmission of ≈90%. The design specifications of the LPDA are given in Table 1.
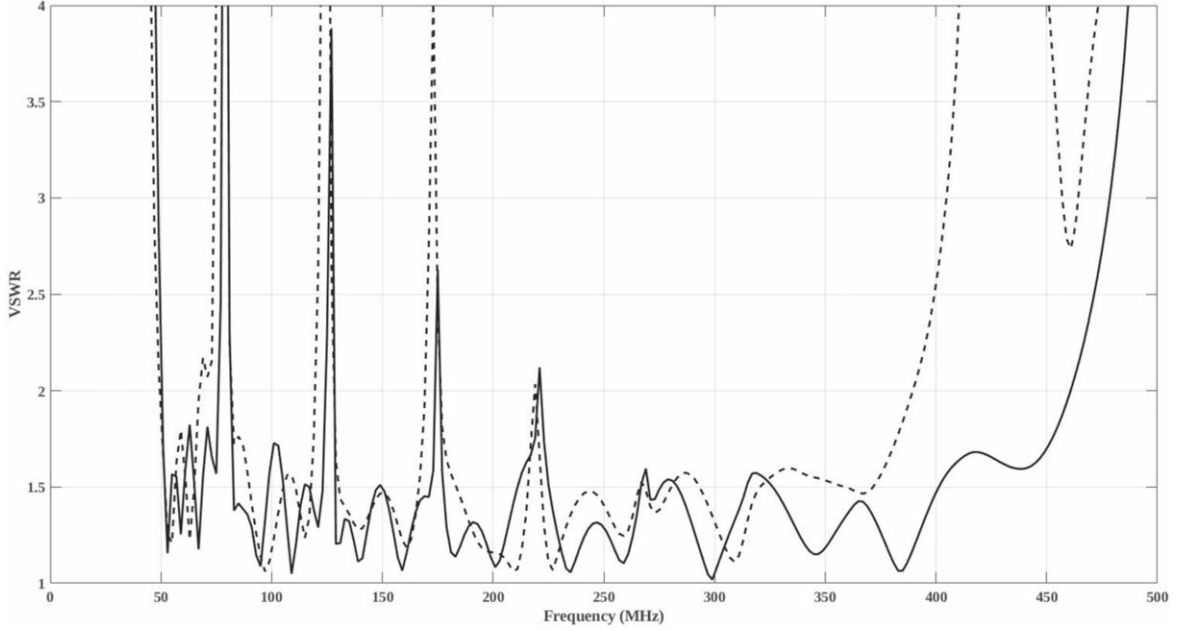

Figure 4. Simulated VSWR using 4NEC2. The dashed and solid lines correspond to the LPDA with 17 and 22 dipoles, respectively.

2.2. New LPDA : Our Design Constraints and Specifications

Having studied the performance of the LPDA extensively, Carrel (1961a) summarized its directional gain (G) as a function of τ and σ (Figure 2). Since we decided to observe the celestial sources for a reasonably long duration and for other technical reasons mentioned in Section 1, a moderate gain of around 6.4 dBi (gain in decibels with respect to an isotropic antenna) was chosen for our prototype LPDA. Further, we wanted to fix an appropriate τ and σ pair to design it; with reference to Figure 2, we could find a range of τ and σ values for a particular gain of the LPDA. In order to select a suitable pair, we varied τ and σ between their lower and upper bounds. This exercise gave us an important input: the dimension of the LPDA grows as τ and σ values are increased. Calculations showed that the dimension of our LPDA could vary from 1.5 m to 5.5 m. In order to minimize the difficulties in handling the LPDA, to optimize the mechanical requirements for mounting it to a rotor for tracking the Sun, and since the length of the longest dipole corresponding to the low-frequency cutoff was about 3 m, it was decided that the largest dimension should be fixed, i.e., the axial length of the antenna should be around 3 m. Additionally, we have kept in mind the anomalous behaviors encountered by Bantin & Balmain (1970) due to large size reduction/compression. These constrained the values of τ and σ to be equal to 0.86 and 0.07, respectively. The total number of dipoles to cover the OB is determined using Equation (3); here, β is the bandwidth ratio.

$$N = \frac{\ln(\beta)}{\ln(1/\tau)}. \tag{3}$$

Table 2
Revision to Table 1 Plus Diameter of Dipoles Used

S. No.	D (cm)	L (cm)	F (MHz)	d (mm)
(1)	(2)	(3)	(4)	(5)
1.	0.0	12.2	614.8	4
2.	3.0	13.7	547.5	4
3.	7.0	15.7	477.9	4
4.	11.0	17.7	423.9	4
5.	15.0	19.7	380.9	4
6.	20.0	22.2	338.1	6
7.	26.0	25.2	297.9	6
8.	32.0	28.2	266.2	6
9.	39.0	31.7	236.8	8
10.	47.0	35.7	210.3	8
11.	56.0	40.2	186.8	10
12.	67.0	45.6	164.3	10
13.	78.0	51.1	146.7	13
14.	91.0	57.6	130.1	13
15.	106.0	65.1	115.2	16
16.	122.0	73.1	102.6	16
17.	141.0	82.6	90.8	19
18.	162.0	93.1	80.6	19
19.	186.0	105.1	71.4	19
20.	212.0	118.0	63.5	19
21.	242.0	133.0	56.4	19
22.	276.0	150.0	50.0	19

Note. Column (2): distance from the apex; column (3): inter-dipole spacing; column (4): half-dipole length ($\lambda/4$); column (5): frequency ($F = c/\lambda$).

Substituting 10 for β and 0.86 for τ, we obtained 15 dipoles for the LPDA; however, since fewer dipoles are usually added (conservative design) to realize the OB of the LPDA, we decided to prepare our prototype with 17 dipoles. The lengths of, e.g., the dipoles and inter-dipole spacing used are listed in Table 1. Two aluminum square tubes (called booms), each having 25 mm × 25 mm sides, 4 mm wall thickness and 3 m length, are used as transmission lines; they are tied apart by 20 mm uniform inter-boom spacing (denoted as "S" in Section 2.4.2) with the help of insulators (or spacers) fixed at several locations along the boom. Aluminum cylindrical tubes of 13 mm diameter are used as dipoles and are fitted to the transmission lines using stainless steel screws, as shown in Figure 1. They are welded to the transmission line in the final design in order to avoid corrosion, etc. A feed-connector is fitted on the top side of the booms. The bottom side of the booms are shorted. A 3.2 m length LMR-200 coax cable running through the grounded-boom is used as the feed cable.

2.3. The Impedance of the LPDA

After the fabrication of the LPDA, its VSWR (voltage standing wave ratio), an indirect measure of impedance, was measured using a vector network analyzer; Figure 3 shows the values as a function of frequency. It is clear that the values, over more than half of the OB, are above 2.0, the value corresponding to a power transmission of about $\approx$90% between the source and the load. To understand the observed trend, we compared the results of the experiments that were carried out to study the performance of LPDAs by varying the OB and design parameters, which are as follows: First, the impedance of the LPDA begins to approach the characteristic impedance

($Z_0 = 50\,\Omega$) throughout its OB when τ and σ values are close to or greater than those of the optimal design curve shown in Figure 2. Second, the VSWR spectrum becomes flat within the intended bandwidth if LPDAs are designed for slightly larger intended bandwidth. Third, the large value of τ and σ increases the dimension of the LPDA as mentioned earlier. From Figure 2, it can be seen that our selected parameter pair lies close to the lower edge of the 6.4 dBi gain-curve. Therefore, the impedance of the prototype LPDA may not lie close to Z_0, and consequently the weak cosmic signals cannot be received by it effectively throughout the OB.

In order to improve the reception efficiency, we decided to bring down the VSWR values below 2.0 over the entire OB. We elaborate on this procedure in Section 2.4 below.

2.4. Fine-tuning the Impedance

To comprehend the variation of impedance of the prototype LPDA, with respect to frequency, simulations were performed. Due to budgetary constraints, the open-source visualization, optimization, and sweeping tool 4NEC2[7] (Burke & Poggio 1981) was used for the simulations. The dashed line in Figure 4 shows the simulated VSWR for the LPDA with 17 dipole elements. Here again, it is clear that the VSWR values increase and exceed 2.0 beyond 375 MHz. The difference between Figure 3 and the dashed-line profile in Figure 4 could be attributed to the limitations and approximations associated with the open-source 4NEC2 as mentioned by Baker & Reuss (1990). However, we continued the simulation further and found that the high values of VSWR above 400 MHz got reduced below 2.5, when the high-frequency cutoff was slightly increased from 555.6 MHz (conventional design value) to 614.8 MHz. Also, the spectrum became flat when the number of dipoles was increased from 17 to 22 within the OB, by slightly altering the design constants as mentioned earlier; moreover, this approach has reduced the VSWR values at 78, 125, and 175 MHz as can be seen from the comparison of the two VSWR profiles in Figure 4. The corresponding revised specifications of the LPDA with 22 dipole elements, used in the simulations, are given in Table 2 (except for the last column). The above process is equivalent to making an LPDA whose design bandwidth is equal to $\approx$1.25 times that of the OB, i.e., $\left(N = \frac{\ln(1.25\,\beta)}{\ln(1/\tau)}\right)$, as pointed out by Karim et al. (2010); the revised τ and σ are equal to 0.89 and 0.06, respectively. However, we note that the revised τ and σ values would not result in the exact values given in Table 2.

Having done the above, trial tests were further continued manually, due to the limitations of the simulation software, to bring down the VSWR below 2.0 throughout the OB. The results of these various tests enabled us to understand that the properties of both transmission line and half-wave dipoles that constitute the LPDA play an important role in deciding its overall impedance (Stutzman & Thiele 1981; Peixeiro 1988; The ARRL Antenna Book 1991); the following subsections deal with them individually.

2.4.1. Selection of Dipoles

For broadband operation of an LPDA, choosing the right set of resonating dipole elements (i.e., with appropriate dimensions) is important since the location of active centers of
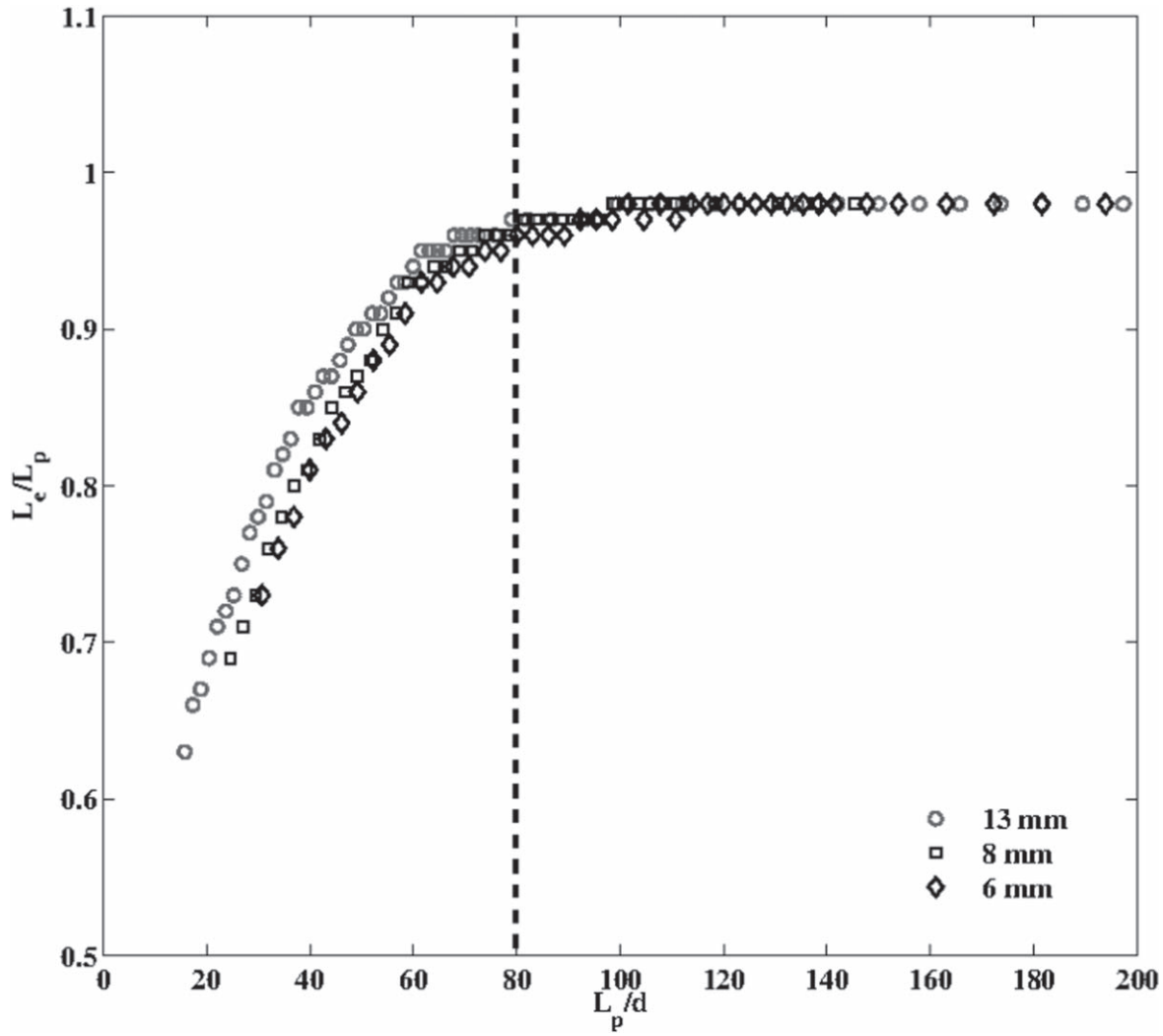
---

[7] https://www.qsl.net/4nec2/

Figure 5. The ratio of electrical length (L_e) to physical length (L_p) of a dipole is plotted against the ratio of its physical length to diameter (d). Measurements taken with aluminum cylindrical tubes of outer diameter 13, 8, and 6 mm are shown with the "circle," "square," and "diamond" symbols, respectively. A vertical dotted line is drawn at $L_p/d = 80$, in order to show that L_e/L_p approaches unity asymptotically beyond that.
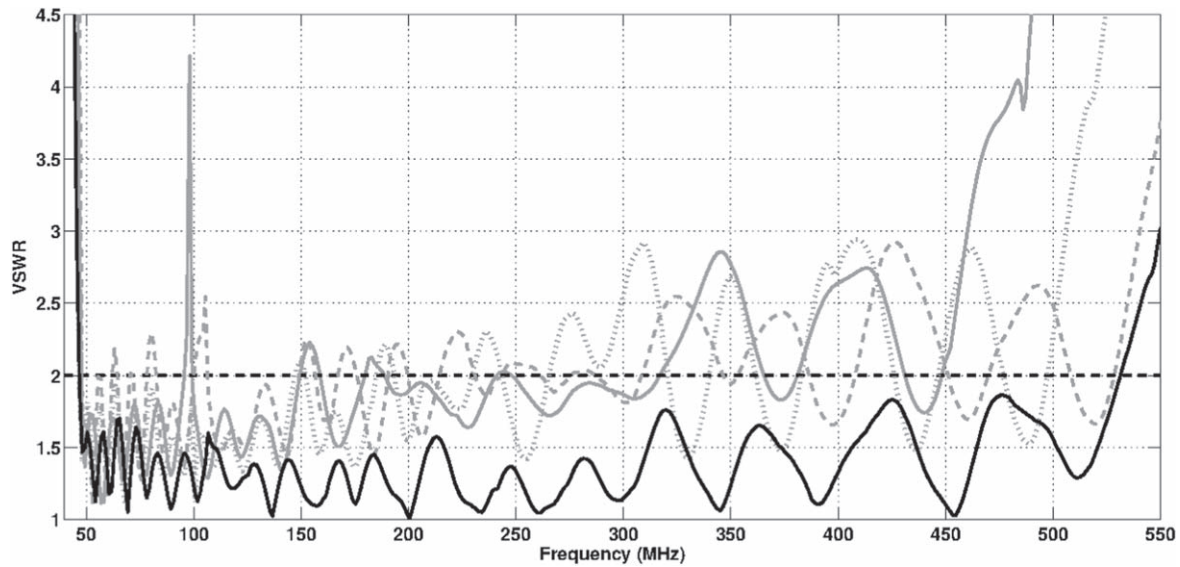

Figure 6. The measured VSWR profiles of the 50–500 MHz prototype LPDA. Solid-gray line: response with design specification as given in Table 1. Dotted-gray line: response with design specification (except the last column) as given in Table 2. Dashed-gray line: response after implementing the suggestion given in Section 2.4.1. Solid-black line: response after implementing the suggestions in Sections 2.4.1 and 2.4.2.
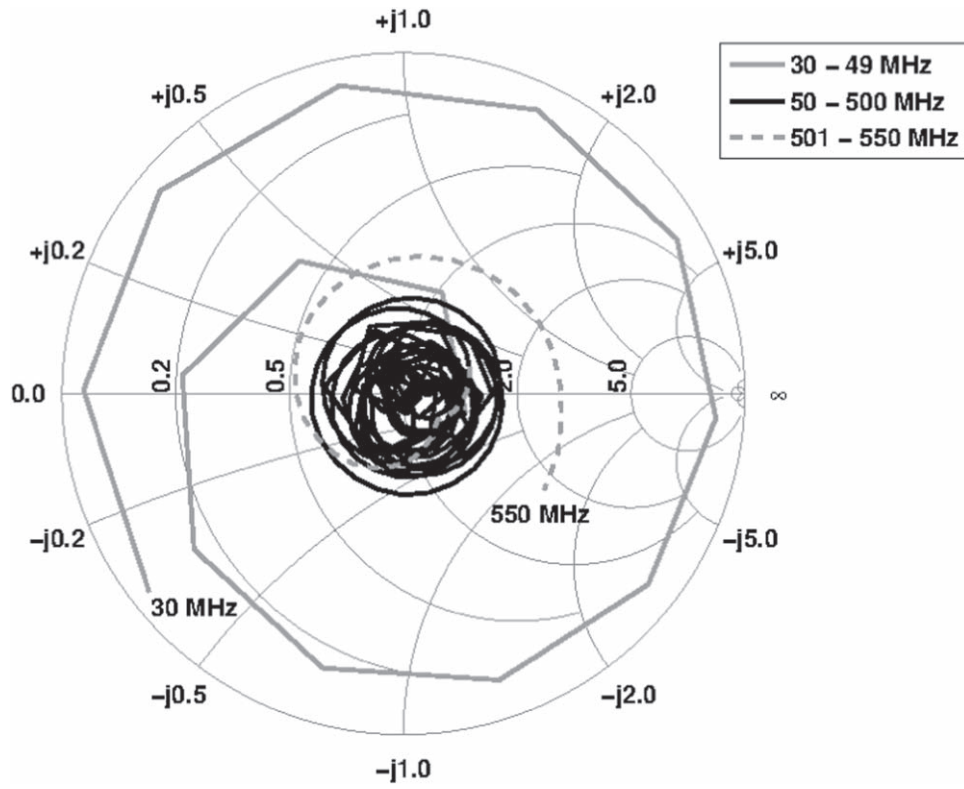
Figure 7. Smith chart of the prototype LPDA after introducing dipoles of different diameters and adjusting the inter-boom spacing; the corresponding parameter values are listed in Table 2.
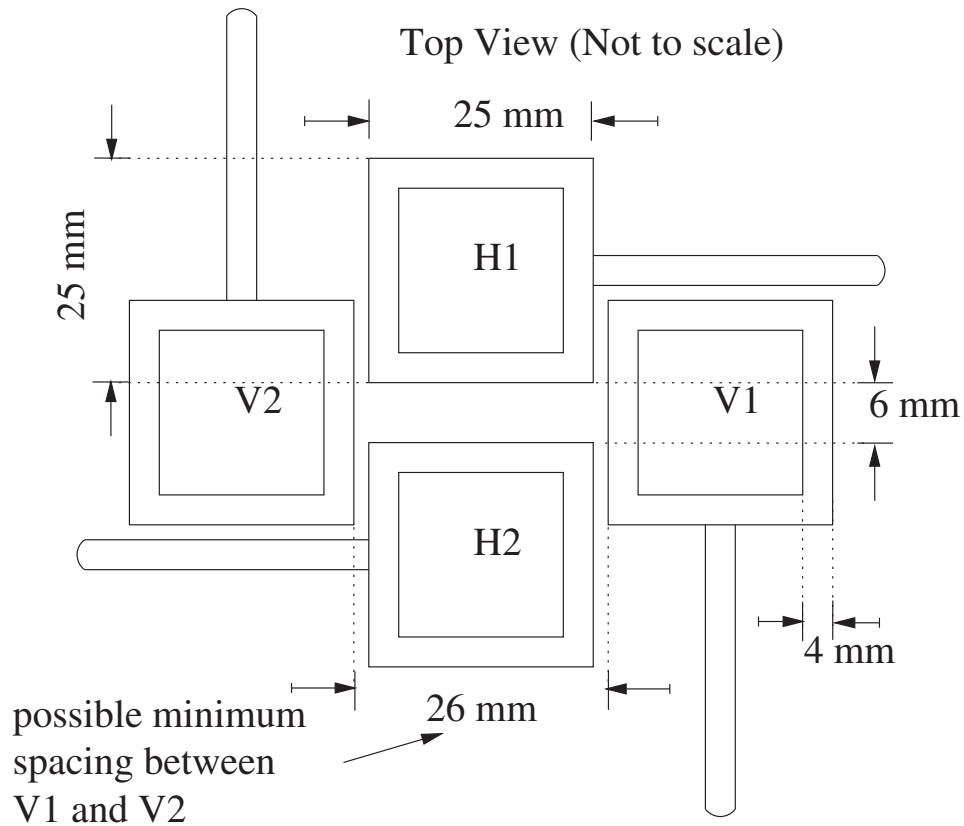

Figure 8. Schematic of the CLPDA with boom transmission lines; the H1 and H2/V1 and V2 pair holds the dipole elements oriented horizontally (X-pol.)/vertically (Y-pol.).
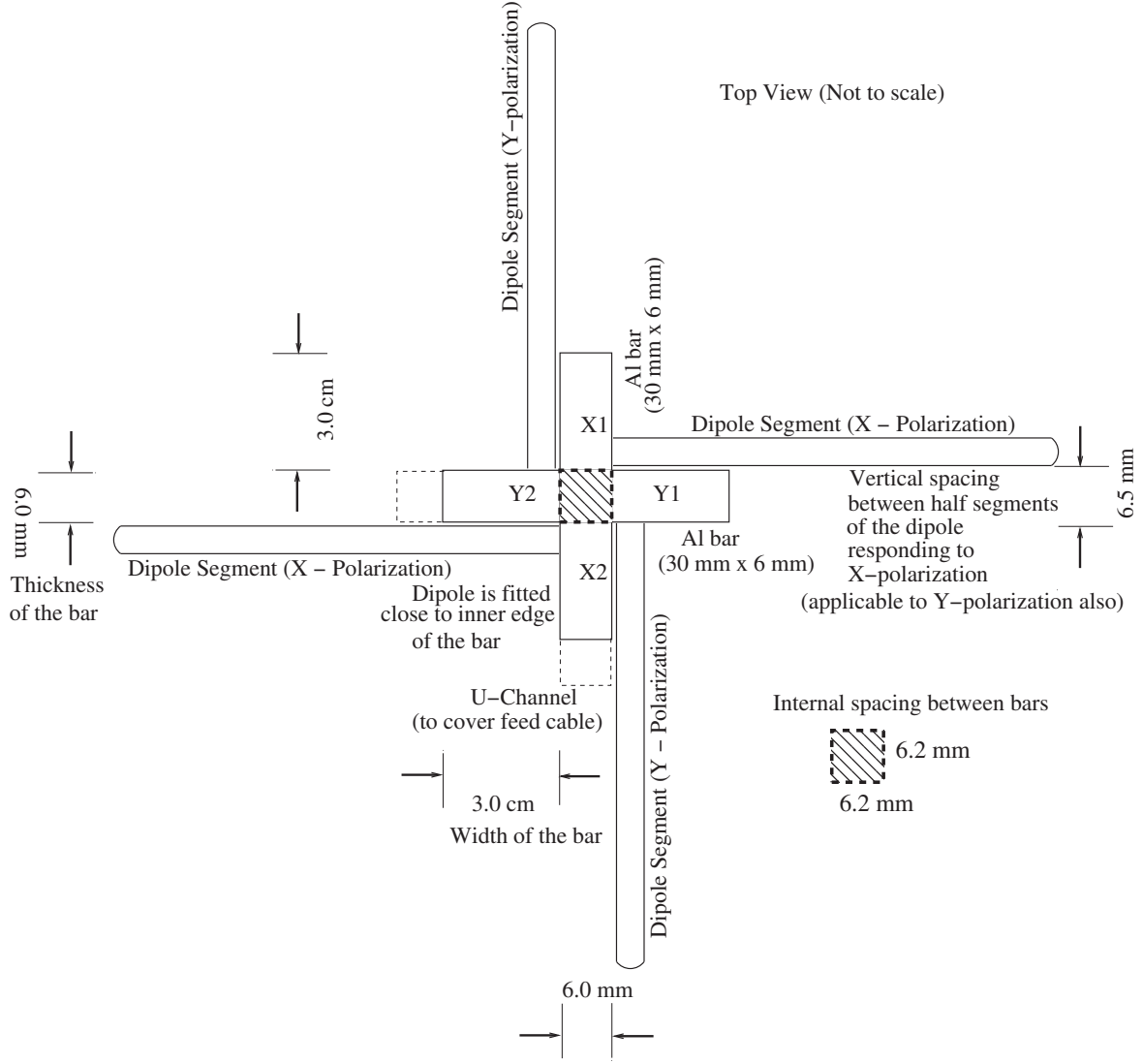
Figure 9. Schematic showing top view of the CLPDA with rectangular bar transmission lines; the X1 and X2/Y1 and Y2 pair holds the dipole elements oriented horizontally/vertically.

reception/transmission moves with frequency (Kraus 1950; Carrel 1961a). The frequency at which a half-wave dipole element resonates depends on its electrical dimension, which in turn is related to its physical dimension. In order to select the right set of dipoles that would work in the OB, we studied the half-wave dipole response alone for various physical lengths and diameters. Aluminum tubes of three different outer diameters, viz. 13, 8, and 6 mm, were used to perform the tests. The result, L_e/L_p versus L_p/d, is shown in Figure 5, where L_e, L_p, and d are the electrical length, physical length, and diameter of the half-wave dipole, respectively. In all of the cases, it can be seen that L_e/L_p varies almost linearly with L_p/d for values $\lesssim 80$; beyond that, the electrical length of a half-wave dipole is almost equal to its physical length, because L_e/L_p approaches unity asymptotically. The latter point was used effectively to fine-tune the impedance of the prototype LPDA: sets of dipoles whose diameter satisfied the above criterion over the OB were selected to construct the LPDA. Aluminum tubes of different diameters (4–19 mm) available to us were used to cover the above bandwidth; although the correct dimensions of the dipoles are required, the nearest

available dimensions are used, as the L_p/d ratio has a moderate influence on the design parameters (Peixeiro 1988). The last column of Table 2 contains the exact diameter of dipoles used to construct the LPDA. The VSWR profile of the LPDA, after the latest changes made, is shown in Figure 6 (gray dashed line). We would like to note here that Bantin & Balmain (1970) used an average L_p/d ratio of 145; the copper rods and the feeder used in their tests gave an impedance of 100 Ω.

2.4.2. Adjusting the Spacing between Transmission Lines

The center-to-center or transverse spacing (S) between the transmission lines of the LPDA plays an important role (Evans 1970; Bantin et al. 1971; The ARRL Antenna Book 1991) in deciding its impedance (Z_{tr}). Equation (4) describes the relationship between the input impedance (Z_i) of the LPDA, impedance of the nearest dipole (Z_d), S, and diameter of the transmission line (D_{tr}).

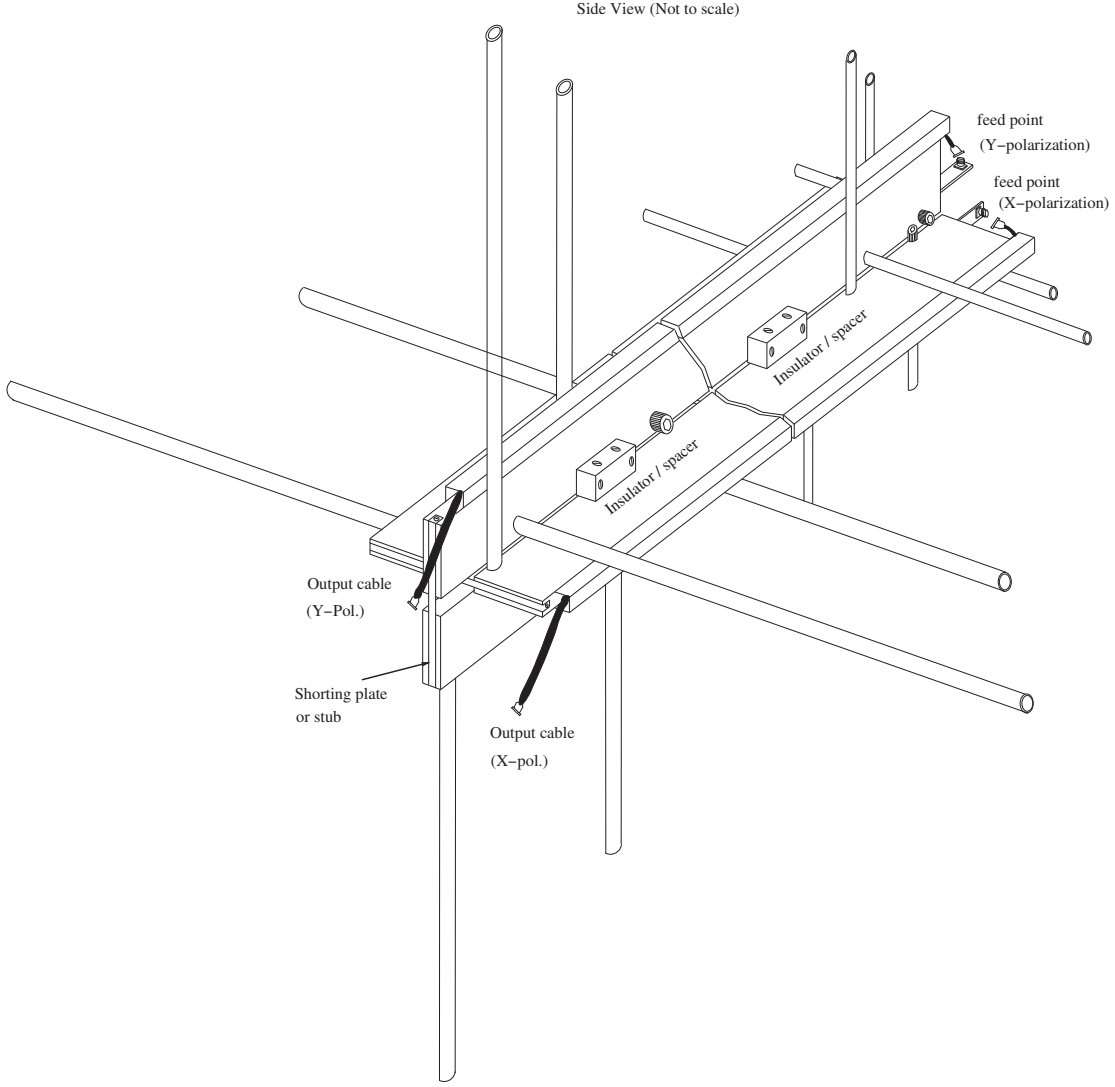$$Z_i = Z_d \log\left(\frac{2S}{D_{tr}}\right). \tag{4}$$

Figure 10. Same as Figure 9, but shown from the side view.

The impedance of the dipole (Z_d) mentioned in Equation (4) depends upon the length (l_n) and diameter (d_n) of the dipole (Equation (5); De Vito & Stracca 1974; The ARRL Antenna Book 1991).

$$Z_d = 120\left(\ln\left(\frac{l_n}{d_n}\right) - 2.25\right). \qquad (5)$$

Since we maintained the length-to-diameter-ratio of dipoles used in our design as constant (≈ 80), the actual values of Z_d would have lain close to each other. Therefore, Z_i in Equation (4) would directly depend upon S, because D_{tr} was also kept constant in our design; this gave us an understanding that the increasing trend of Z_i from low-frequency cutoff to high-frequency cutoff as seen from the gray dashed line of Figure 6, could have been due to a progressive increase in S (above the required value) toward the high-frequency side; since the existing S was a constant (20 mm throughout), the tests were continued by decreasing S more (up to 5 mm) toward the high-frequency side. As expected, this approach brought down the VSWR well below 2.0 throughout the OB, which

resulted in overall matching of impedance (with Z_0) of the prototype LPDA. However, by varying the gradient of S, the configuration that yielded the lowest mean VSWR was identified. The one that had 6 mm close to the location of 500 MHz dipole and 60 mm close to the location of 50 MHz gave rise to 1.35 as mean VSWR. The solid-black profile shown in Figure 6 was obtained after adjusting S; its corresponding Smith chart is shown in Figure 7, and one can see that the normalized impedance values lie well between 0.5 and 2.0 in the OB. This result is in agreement with Bantin & Balmain (1970) for the size-reduced or compressed LPDA configuration. Further, the authors report a shift in the low- and high-frequency cutoff of the design bandwidth of the LPDA for the compressed configuration when $\alpha \gtrsim 30°$. This is possible because the present prototype does not show any such shifts, since α is around 28° in our case. At the same time, we would like to note that our result does not show any break-out frequency in the impedance profile for the compressed case as shown in Bantin & Balmain (1970). The back-lobe level anomalies are avoided since $\tau = 0.89$ as mentioned in Bantin et al. (1971). Kyei & Jung (2018) concludes that the length
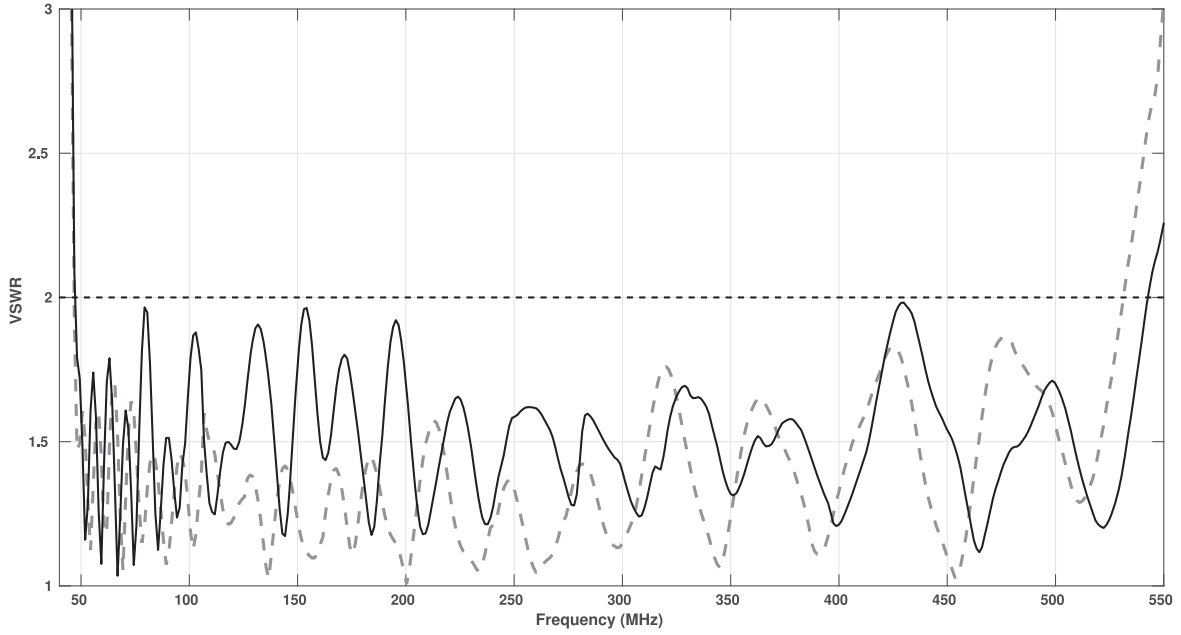
Figure 11. The solid-black profile is the measured VSWR of the prototype CLPDA. The dashed-gray profile, the measured VSWR of the 50–500 MHz prototype LPDA (the same as the solid-black profile of Figure 6), is overplotted for the sake of comparison.

reduction of an LPDA by decreasing the spacing factor and increasing the number of dipoles would lead to a 58% reduction in OB. However, such an effect is not noticed in our tests. Thus, the above impedance values indicate that the LPDA can receive the radio waves in the OB effectively. Also, it must be emphasized that neither a 2:1 nor a 4:1 impedance transformer (BALUN) nor a resistive stub (Bantin et al. 1971) was used anywhere to match the impedance of the LPDA with Z_0, as is generally followed. Further, during the tests, it was found that similar VSWR response in the OB could be obtained by joining the transmission lines using an insulated-wire-stub of length $\frac{\lambda_{max}}{8}$; for compactness, the stub may be made into a coil; in such a case, the number of dipoles required to realize the OB with a coil-stub configuration would be lesser than the one without that. The reduction in the number of dipoles depends upon the design parameters; it is equal to five for the present prototype LPDA. Although this result seems interesting, it has to be verified thoroughly using coil-stub prototypes with different OB ratios. Therefore, the prototype without the coil-stub was used further for the fabrication of the CLPDA.

3. Fabrication and Characterization of the CLPDA

As mentioned in the beginning of Section 2, a CLPDA was constructed by fitting two LPDAs with dipole-orientations orthogonal to each other with vertical axes being the same. Followed by the LPDA fabrication, a schematic was drawn (Figure 8) as a part of the preparatory work to the CLPDA; while drawing, it was realized that constructing a CLPDA using a boom type transmission line would not help because the transmission lines of the orthogonal components of the CLPDA should be separated by 6 mm at the top; an inspection of Figure 8 indicates that though the latter is achievable for one of the components (H1 and H2), it is not for the other (V1 and V2), since the dimension of the boom (25 mm × 25 mm)

would be larger than the spacing required (i.e., 6 mm × 6 mm). Naturally, the dimension of the transmission line was constrained to be equal to 6 mm × 6 mm; yet, since the prototype LPDA was prepared using dipoles having different diameters (4–19 mm), the dimension of the transmission lines had to be increased from 6 mm × 6 mm to 6 mm × 30 mm (Figure 9) in order to fit those dipoles onto the CLPDA transmission lines. Therefore, the transmission line pairs (X1–X2 and Y1–Y2) of the CLPDA were prepared out of slender (6 mm thickness × 30 mm width) aluminum rectangular bars instead of the previously used 25 mm × 25 mm booms (with 4 mm wall thickness). A rectangular bar was preferred to a rectangular tube for better rigidity since it should run for a length of 3 m. Each transmission line pair was fitted with a "U" channel to the outer edge of one of the pair (X2 and Y2) to run the feed cable through it; two separate RG-58 coax cables, each having a length of 3.2 m, were used to tap the signal from the feed connectors fitted to X1–X2 and Y1–Y2 pairs, respectively (Figure 10); the latter pairs can be oriented such that the first one receives the horizontal component and the second one receives the vertical component of the polarized signal falling on them. Before proceeding with the preparation of the CLPDA, we took into account the suggestions given in Pivnenko (2006), which state that the spatial separation between the transmission lines of an LPDA/a CLPDA at a particular location must be $\lesssim \frac{1}{100}$ times the wavelength of operation of the nearest dipole for restricting the electromagnetic field vibrations within a very narrow cone angle. This was recommended to minimize the polarization leakage and thereby to detect the state of polarization, presumably with better precision. Therefore, an insulator of dimension 6.2 mm × 6.2 mm × 100 mm (width × height × length) was carefully fitted between two orthogonal components of transmission lines at several locations to ensure that the spacing between the transmission line at any location satisfies Pivnenko's criterion; also, the dipoles were fitted close to the
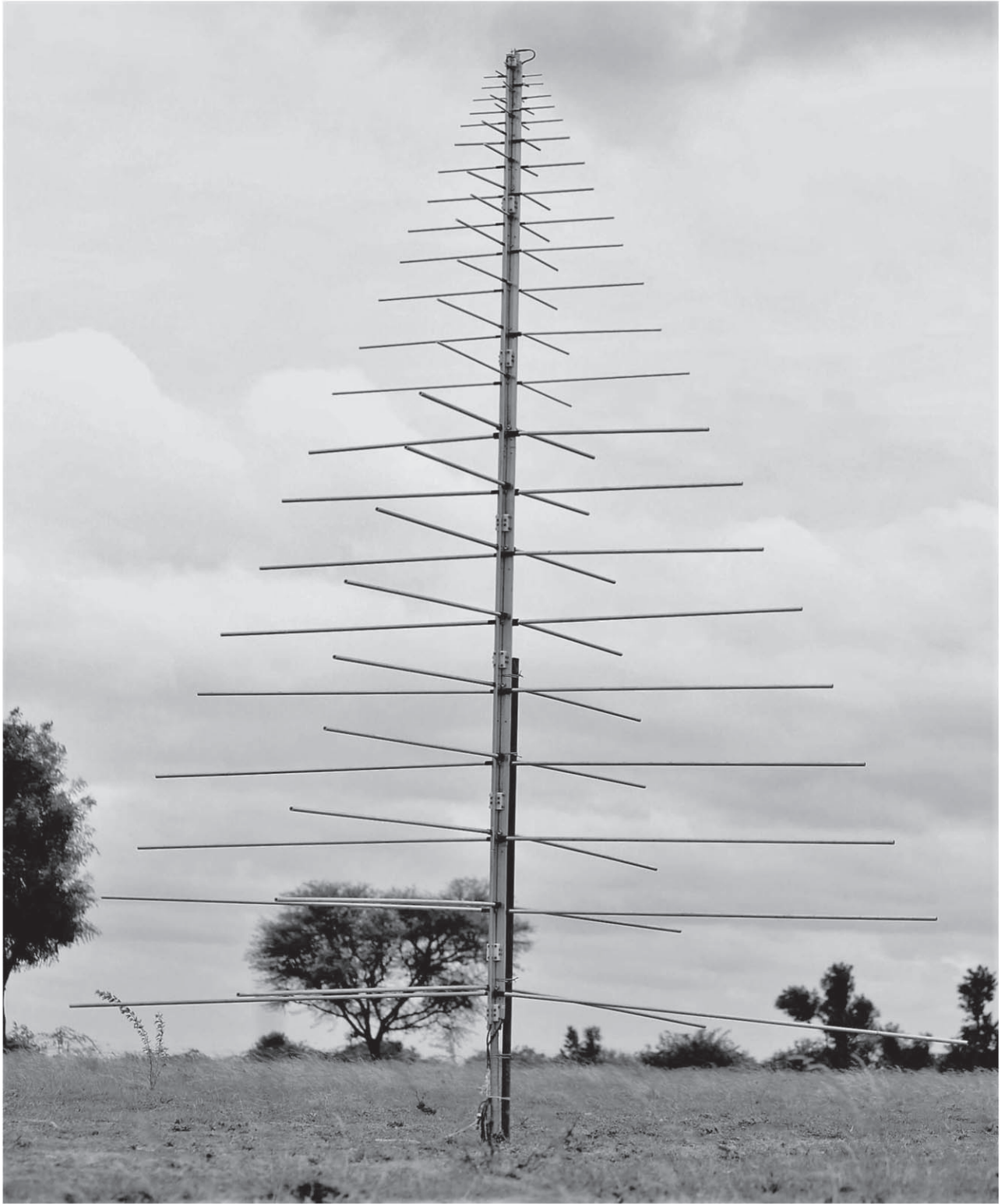
Figure 12. Photograph of the prototype CLPDA.

inner edge of the rectangular bars so that the vertical spacing between the half segments that constitute a dipole is almost equal to the spacing between the transmission lines, which is equal to 6.5 mm (Figure 9), at the location of the dipole. Additional spacers were also fitted to vary the inter-transmission line spacing from about 6.5 to 60 mm. The location, inter-dipole spacing, and diameter of the dipoles given in Table 2 were followed again in fabricating the prototype CLPDA. The VSWR was measured for it, and the values were found to be below 2.0 throughout the OB. As was done earlier, the gradient in the inter-transmission line spacing was varied to identify the configuration that would give the lowest average VSWR; the CLPDA configuration, which had 6.5 mm spacing at the top and 30 mm at the bottom gave 1.52 as the lowest; the solid-
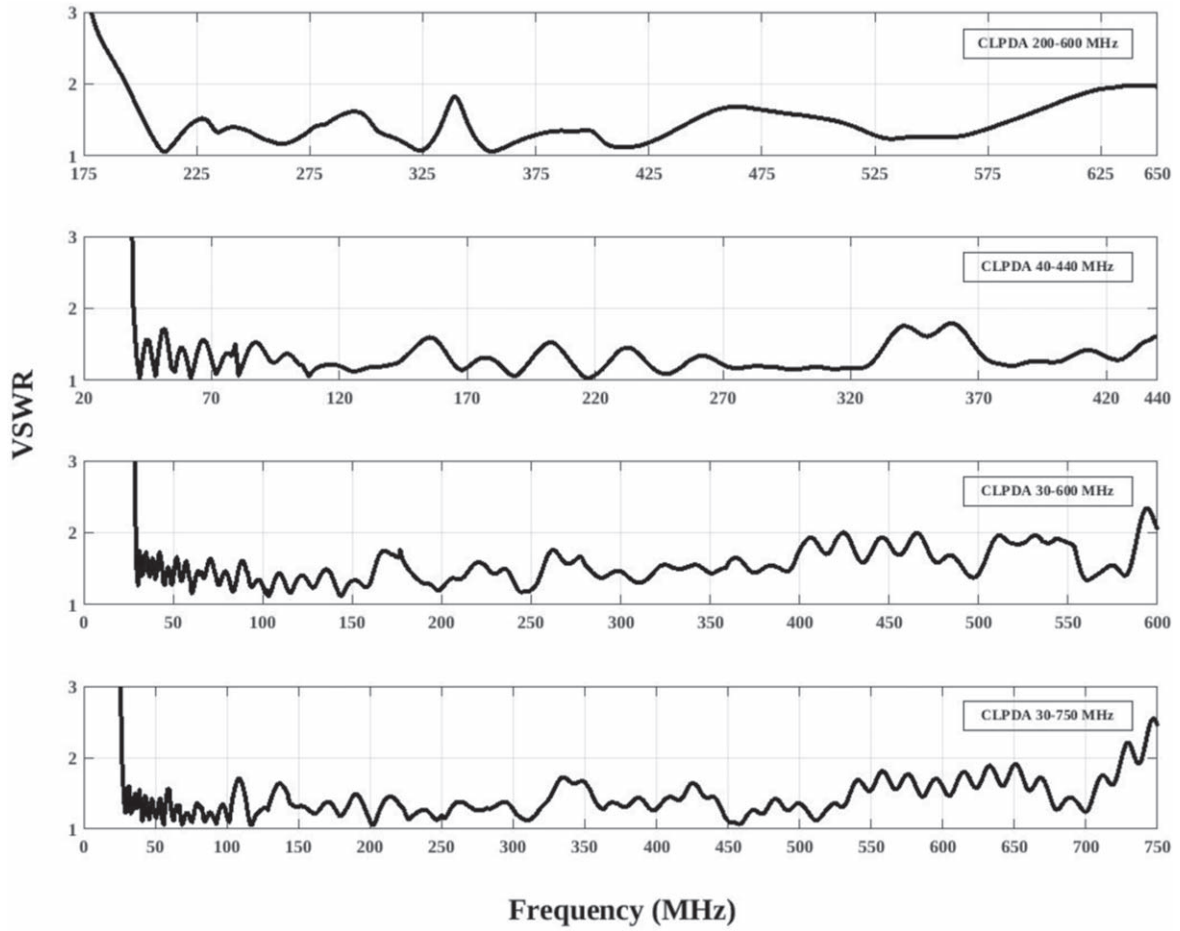
Figure 13. Top to bottom: VSWR profiles of the prototype CLPDAs having OB ratios 1:3 (200–600 MHz), 1:11 (40–440 MHz), 1:20 (30–600 MHz), and 1:25 (30–750 MHz).

Table 3
Measured CLPDA Parameters

S. No.	Parameter	Value
1.	HPBW (E)	$\approx 65°$
2.	HPBW (H)	$\approx 100°$
3.	Gain	≈ 6.6 dBi
4.	Effective collecting area	$\approx 0.4\ \lambda^2$
5.	Front to back ratio	≈ 30 dB
6.	Side lobe ratio	≈ -24 dB
7.	Polarization isolation (mean)	≈ -30 dB

black profile shown in Figure 11 is the measured VSWR of the CLPDA. For comparison, the solid-black profile of Figure 6 has been overplotted, but in a gray dashed-line form. The photograph of the CLPDA is shown in Figure 12. It is clear from Figure 11 that the VSWR of the CLPDA, and hence its impedance, differs from the prototype LPDA; this difference is most likely due to different transmission lines used to fabricate them, as the rest of the components used are the same for both antennas. With the open-source 4NEC2 software, we were unable to carry out the simulations to understand the effects of using different types of transmission lines and their actual mechanical structure, dimensions, etc., since it has limitations. However, in the near future, we would like to procure one of the modern sophisticated commercial software packages such

as CST[8] microwave studio, IE3D,[9] HFSS,[10] and Super-NEC (Fard 2011) for the simulation studies. The results of those exercises could be close to the experimental values due to reasons mentioned in Cheong & King (1967); these shall be summarized in a forthcoming article. Further, it must be noted here that the prototypes with different OB ratios viz. 1:3 (200–600 MHz), 1:11 (40–440 MHz), 1:20 (30–600 MHz), and 1:25 (30–750 MHz) were also designed, fabricated, and tested to study the applicability of this new procedure. The test results were satisfactory (Figure 13); the average VSWR of the above prototypes were 1.37, 1.31, 1.52, and 1.41, in their respective OB. Also, the difference between the operating frequency of the top dipole of the conventional CLPDA/LPDA (Table 1) and the one designed using the new procedure (Table 2) is about 60 MHz, whereas it is <10 MHz for the above different OB prototypes. Therefore, the new procedure is very effective in obtaining the optimum-design-point in the design-parameter-space, which is in the close vicinity of the conventional-design point. The latter appears to be in agreement with the conclusion by Isbell (1960), which states that the LPDA/CLPDA is essentially frequency independent for certain parameter values. Having been developed, the prototype CLPDA (50–500 MHz) was then tested for its reception characteristics.

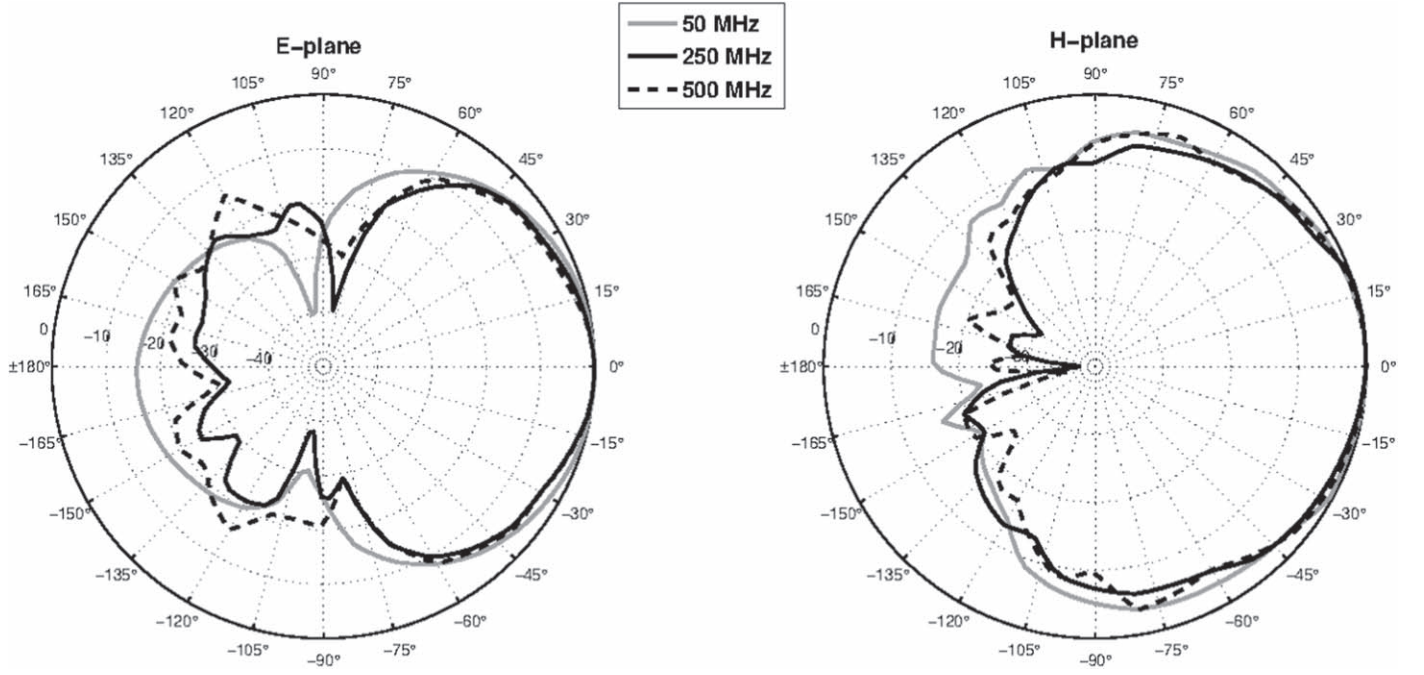[8] https://www.3ds.com
[9] https://www.rfglobalnet.com
[10] https://www.ansys.com

Figure 14. Measured E-plane (left panel) and H-plane (right panel) radiation patterns at 50, 250, and 500 MHz.
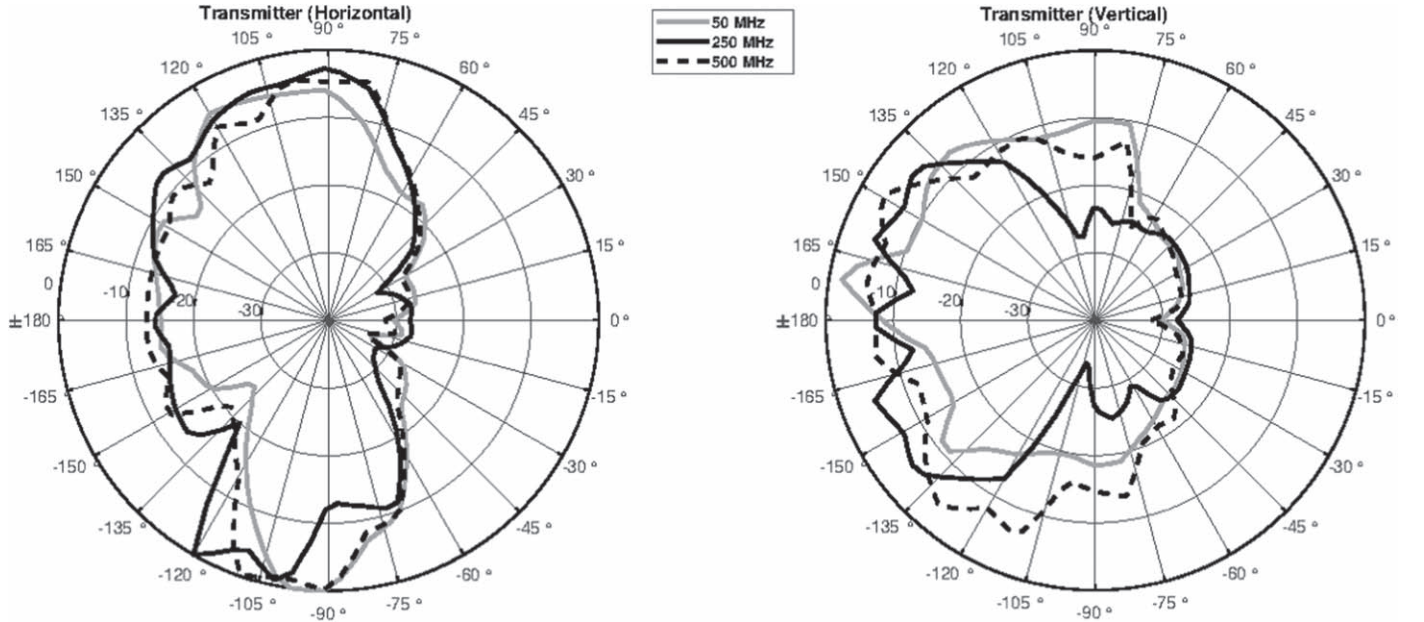

Figure 15. Polarization crosstalk or isolation pattern of the CLPDA at 50 (solid-gray), 250 (solid-black), and 500 MHz (dashed-black). Left: transmitter kept in horizontal orientation. Right: transmitter kept in vertical orientation.

3.1. Radiation Pattern Measurements

The far field radiation pattern was measured by keeping the transmitting and receiving antennas in the theoretical far field distance $\left(R > \frac{2D^2}{\lambda}\right)$; it was equal to 50 m in the actual measurement setup. The designed antenna was used as a receiver, and an LPDA with known transmission characteristic was used as the transmitter. For the measurement of the E-plane radiation pattern, both transmitting and receiving antennas were oriented horizontally, and the receiver antenna was rotated in the azimuthal plane from 0° reference position to 360°; the readings were noted down every 15°. The same procedure was

repeated for measuring the H-plane pattern but with both antennas oriented in the vertical position. The measured average values of the half-power beamwidth (HPBW) of the E-plane and H-plane are 65° and 100°, respectively. The H-plane beamwidth is greater than that of the E-plane with a larger back lobe, as pointed out by Jones & Mayes (1969). Also, it is clear that the frequency-independent characteristics are retained throughout the bandwidth even after the reduction of the transmission-line length (Jones & Mayes 1969; Bantin & Balmain 1970). Other antenna parameters, such as gain and effective aperture area, were deduced from the above and are listed in Table 3. These parameters were found to be constant almost throughout the OB. Figure 14 shows the radiation
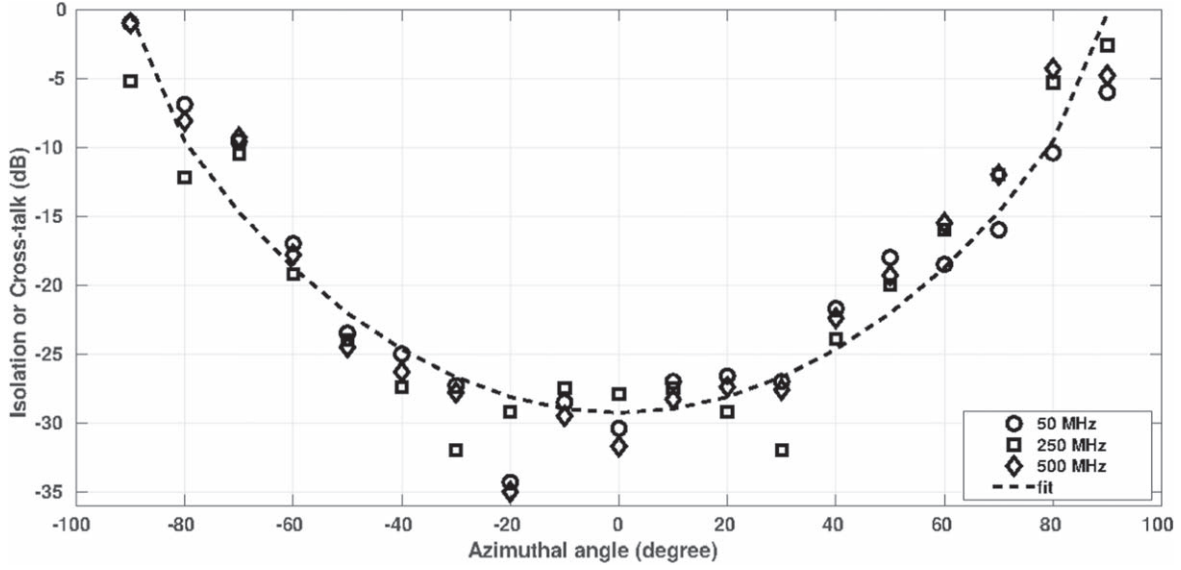
Figure 16. Measured polarization crosstalk of the CLPDA as a function of azimuthal angle when the transmitter was kept in horizontal orientation. The values at 50, 250, and 500 MHz are shown with open circle, square, and diamond symbols, respectively. A custom fit ($-a \cos^b \theta - c$) to the average crosstalk values is shown with dashed marks. The best fit ($\chi^2 \approx 0.93$ and rms error ≈ 2.5) was obtained when the coefficients a, c, and power index b were equal to ≈ 30, 0.3, and 0.65, respectively. The latter gives ≈ -30, -29, -27, -24, -19, -13, and 0 dB as the average crosstalk values at position angles 0°, 15°, 30°, 45°, 60°, 75°, and 90°, respectively.
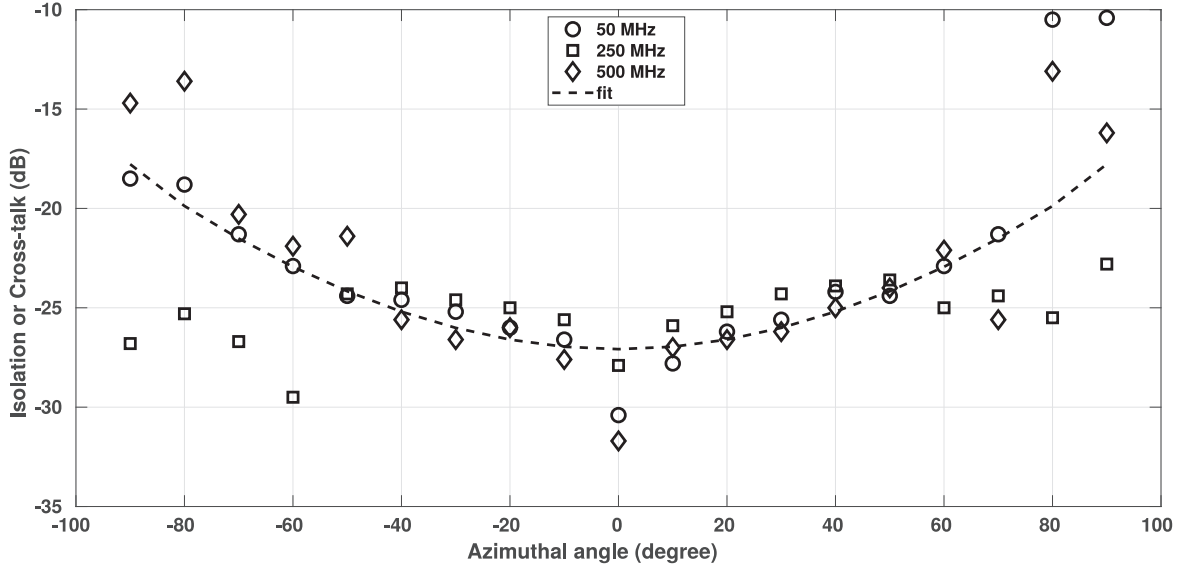
Figure 17. Same as Figure 16 but when the transmitter was kept in the vertical orientation. The best fit ($\chi^2 \approx 0.82$ and rms error ≈ 2.0) was obtained when the coefficients a, c, and power index b were equal to ≈ 9.3, 17.8, and 0.85, respectively. The average crosstalk values are ≈ -27, -27, -26, -25, -23, -21, and -18 dB at 0°, 15°, 30°, 45°, 60°, 75°, and 90°, respectively.

pattern measured at 50 ("solid-gray"), 250 ("solid-black"), and 500 MHz ("dashed-black") for the E-plane and H-plane, respectively.

3.2. Estimation of Polarization Cross-talk

The polarization pattern of an antenna is dependent on its geometry (Stutzman & Thiele 1981). For instance, a helix is circularly polarized whereas a dipole is linearly polarized. Since the primary objective of this study is to measure the circularly polarized radio emission from the Sun using a CLPDA frontend system, restricting the E- and H-fields, within a narrow region about their respective mean positions of vibration, is important. Otherwise, one of the fields will spill over into the other. The magnitude of spillover determines the

uncertainty involved in any parameter deduced from the polarization measurements. The parameter that quantitatively describes this spillover is called the "polarization crosstalk" or "isolation" (Wakabayashi et al. 1999; Pivnenko 2006), a measure of received power corresponding to one sense of polarization by an antenna when it is exposed to a polarized radiation of the other or of the opposite sense. As mentioned above, minimization of this parameter is expected to improve the accuracy with which the degree of circular polarization (DCP) is determined and, consequently, the determination of the magnetic field strength from the DCP. In order to determine the crosstalk, the transmitter was kept in both horizontal and vertical orientations successively, and the signal strengths were measured with both horizontal and vertical arms of the CLPDA. Figure 15 shows the crosstalk or isolation pattern of
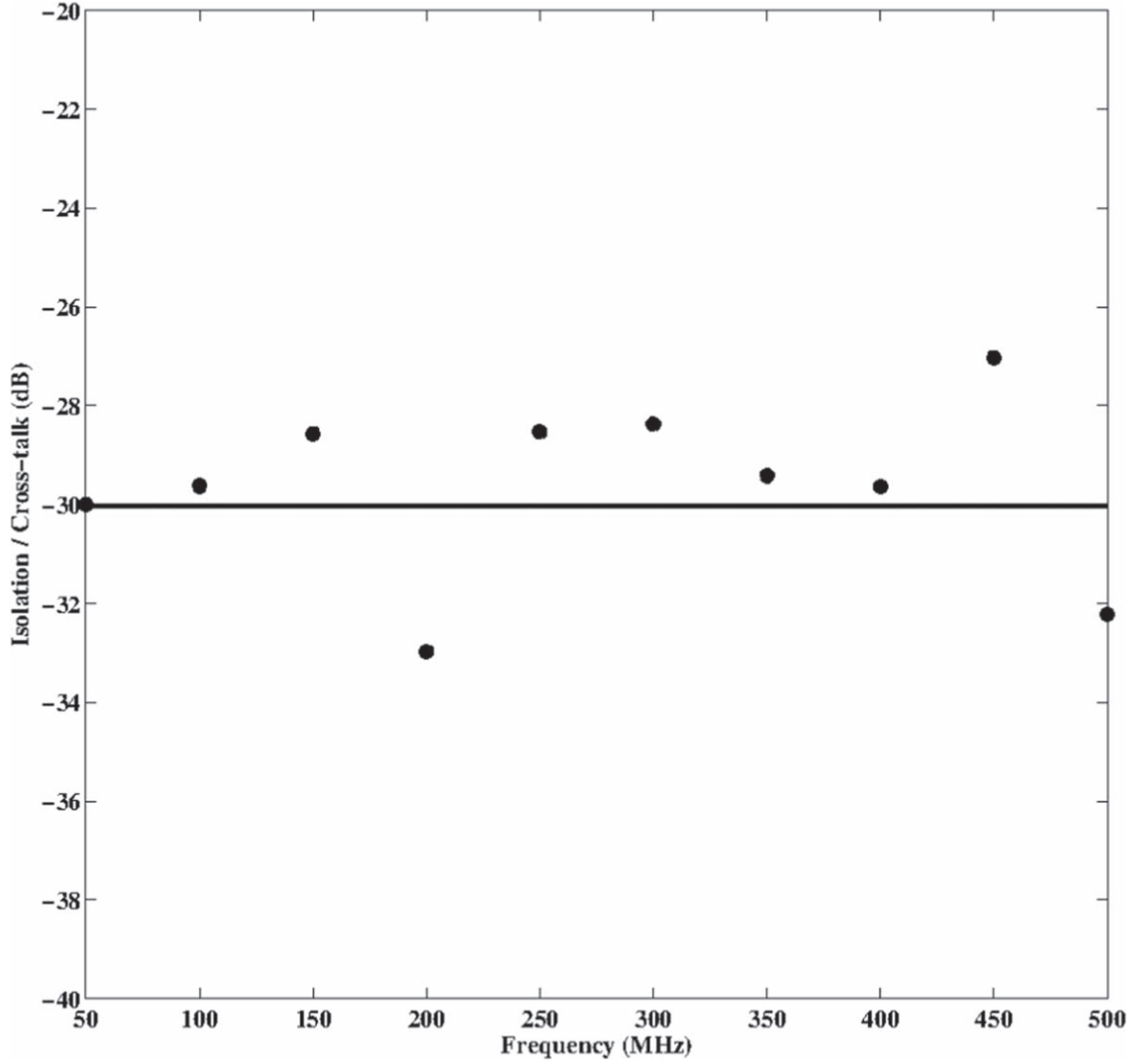
Figure 18. Isolation/crosstalk of the CLPDA at 0° azimuthal angle vs. frequency. The "filled circle" symbols correspond to the measured crosstalk level at different frequencies, and the "solid-black" line represents the mean value.

the CLPDA at different frequencies; the left (right) panel corresponds to the CLPDA response when the transmitter was kept in horizontal (vertical) orientation. The profiles show a minimum of −36 dB (at 500 MHz) and a maximum of −20 dB (at 50 MHz) within the ±60° azimuthal angle from the reference position (0°, i.e., the direction of maximum transmission of the transmitter). Since we planned to observe the sources for about 3 hr on either side of the local meridian and for different declinations, the average crosstalk as a function of azimuthal angle was determined for both orientations (horizontal and vertical) of the transmitter; custom fits to the crosstalk values are shown in Figures 16 and 17, respectively. A comparison of these two figures indicates that the crosstalk values, within ±45°, are lower for the case in which the transmitter was kept in horizontal orientation as compared to the other case. This is due to (i) the maximum reception of the E-field and (ii) the maximum rejection of H-field by the CLPDA within that azimuthal angular span. Whereas the crosstalk increases beyond that in the horizontal transmitter case due to increase in reception of the H-field as compared to the E-field. Also, the overall difference in

crosstalk distribution, as a function of azimuthal angle, between the transmitter kept in horizontal and vertical orientation, is most likely due to the difference in the reception pattern of orthogonal components of the CLPDA.

The crosstalk values at 0° position alone were plotted as a function of frequency and are shown in Figure 18; their average value is about −30 dB. This is about 10 dB lower than those that are available commercially; the majority of the latter use booms as transmission lines. We are interested in reducing the back lobes further in our future design so that the crosstalk can be minimized further over angles $\gtrsim \pm 60°$. We note here that Evans (1970) demonstrated that the radiation pattern for feed displacements $\lesssim \frac{2}{100} \lambda$ retains the symmetrical center-fed dipole characteristics and would lead to an increase in side-lobe levels if the design exceeds that condition.

4. Discussions and Conclusions

We designed and fabricated a CLPDA that works in the 50–500 MHz frequency range; the design constraints, the procedure to tune its impedance, and the procedure to

moderately minimize its dimension are explained. Throughout the OB, the CLPDA has a directive gain of about 6.6 dBi, return loss $\lesssim -10$ dB, and a polarization leakage or crosstalk $\lesssim -27$ dB at the reference position angle (i.e., azimuthal angle = 0°). The latter is about 10 dB less than the commercially available ones; this is due to the adoption of Pivnenko's criterion (Pivnenko 2006). According to the latter, a significant reduction in the cross-polarized field can be obtained by placing the two arms of each dipole (of an LPDA) avoding the vertical displacement and preferably in the same plane. The vertical displacement maintained between the two arms of the dipoles in his prototype LPDA was equal to $\frac{1}{100}$ th of the arm length. The latter was achieved by use of rectangular bars (as transmission lines) instead of the generally used square tubes to fabricate the LPDA/CLPDA. The variation of the crosstalk as a function of azimuthal angle (θ) was also measured for the transmitter kept in both horizontal and vertical orientations; the custom fit to the mean crosstalk values follow the form $\cos^b \theta$, where b is equal to 0.65 and 0.85, respectively. Although the space is not a constraint for the present observing setup, keeping in mind our future plan of setting up a tracking system, reducing the axial and transverse dimensions of the CLPDA further, would be ideal to minimize the weight of it and other related handling issues. Similar methods described in Chen et al. (1994) may be evolved to optimize the radiation patterns of the CLPDA designed using fractalization techniques without affecting the other parameters and that too for large bandwidth ratios. This could be achieved by carefully fusing new ideas with the modern miniaturization techniques mentioned in Section 1. Use of one of the modern simulation packages such as the CST microwave studio, IE3D, HFSS, Super-NEC, finite element method, etc. would be helpful to realize our goal. As previously mentioned, an in-depth exploration of the configuration of the SP receiver setup will follow this article in future work.

Acknowledgments

ORCID iDs

Anshu Kumari ⓘ https://orcid.org/0000-0001-5742-9033
C. Kathiravan ⓘ https://orcid.org/0000-0002-6126-8962
R. Ramesh ⓘ https://orcid.org/0000-0003-2651-0204

References

Alissandrakis, C. E., & Gary, D. E. 2021, FrASS, 7, 77
Allaart, M. A. F., Van Nieuwkoop, J., Slottje, C., & Sondaar, L. H. 1990, SoPh, 130, 183c
Allen, C. W. 1947, MNRAS, 107, 386
Anagnostou, D. E., Papapolymerou, J., Tentzeris, M. M., et al. 2008, IAWPL, 7, 456
Antar, Y. M. M., Zavvari, A., Islam, M. T., et al. 2014, IAPM, 56, 278
Aschwanden, M. 2006, Physics of the Solar Corona : An Introduction with Problems and Solutions (Berlin: Springer)
Baker, D. C., & Reuss, T. G. 1990, ITB, 36, 89
Bantin, C. C., & Balmain, K. G. 1970, ITAP, 18, 195
Bantin, C. C., Balmain, K. G., Okes, C. R., & David, L. 1971, ITAP, 19, 286
Benz, A. O., Gudel, M., Isliker, H., Miszkowicz, S., & Stehling, W. 1990, SoPh, 133, 385
Benz, A. O., Monstein, C., Beverland, M., et al. 2009a, SoPh, 260, 375
Benz, A. O., Monstein, C., Meyer, H., et al. 2009b, EM&P, 104, 277
Best, S. R. 2002, IAWPL, 1, 74
Bogod, V. M., Vatrushin, S. M., Abramov-Maximov, V. E., Tsvetkov, S. V., & Dikij, V. N. 1993, in ASP Conf. Ser. 46, The Magnetic and Velocity Fields of Solar Active Regions (San Francisco, CA: ASP), 306
Bolli, P., Mezzadrelli, L., Monari, J., et al. 2020, IEEE Open J. Antennas Propag., 1, 253
Breed, G. 2008, High Frequency Electronics, 7, 50
Burke, G. J., & Poggio, A. J. 1981, Technical Document 116, Naval Ocean Systems Center
Campbell, C. K., Traboulay, I., Suthers, M., & Kneve, H. 1977, ITAP, 25, 718
Cane, H. V. 2002, JGRA, 107, 1315
Carley, E. P., Vilmer, N., & Vourlidas, A. 2020, FrASS, 7, 79
Carrel, R. L. 1961a, in IRE International Convention Record, Part I (New York: IEEE)
Carrel, R. L. 1961b, Technical Report 52, Univ. Illinois
Chen, W., Jen, L., & Zhang, S. M. 1994, ElL, 30, 1264
Cheong, W.-M., & King, R. W. P. 1967, RaSc, 2(New Series), 11, 1267
Chung, Y. C., & Haupt, R. L. 2001, JEWA, 15, 1269
De Groot, T., & Van Nieuwkoop, J. 1968, SoPh, 4, 332
De Lera Acedo, E., Razavi-Ghods, N., Troop, N., Drought, N., & Faulkner, A. J. 2015, ExA, 39, 567
De Vito, G., & Stracca, G. B. 1974, ITAP, 22, 714
DiFonzo, D. F. 1964, Microwave J., 7, 37
Du, Q.-F., Chen, L., Zhao, Y.-C., et al. 2017, RAA, 17, 98
DuHamel, R., & Isbell, D. 1966, in 1958 IRE International Convention Record (New York: IEEE), 119
Dumas, G., Caroubalos, C., & Bougeret, J.-L. 1982, SoPh, 81, 383
Ebenezer, E., Subramanian, K. R., Ramesh, R., et al. 2007, BASI, 35, 111
El-Khamy, S., Mangoud, M., Aboul-Dahab, M., et al. 2004, in Proc. IEEE Antennas and Propgation Society Int. Symp. (New York: IEEE), 3433
Ellingson, S. W., Clarke, T. E., Cohen, A., et al. 2009, IEEEP, 97, 8
Evans, B. G. 1970, ITAP, 18, 124
Fard, F. M. 2011, Int. J. Mach. Learn. Comput., 1, 311
Fu, Q., Ji, H., Qin, Z., et al. 2004, SoPh, 222, 167
Gary, D. E. 2008, arXiv:1901.09262
Geethan, A. A., & Anagnostou, D. E. 2008, in IEEE Antennas and Propagation Society Int. Symp. (New York: IEEE),
Gong, B., Su, L.-H., Yin, Y.-Z., Ma, H., & Zheng, Q.-R. 2012, in 2nd Int. Conf. in Consumer Electronics and Networks (New York: IEEE), 61
Gopalswamy, N., & Kundu, M. R. 1987, SoPh, 111, 347
Greiser, J. W. 1964, IEEEP, 52, 617
Grognard, R. J.-M., & McLean, D. J. 1973, SoPh, 29, 149
Hamini, A., Auxepaules, G., Biree, L., et al. 2021, JSWSC, 11, 57
Hariharan, K., Ramesh, R., & Kathiravan, C. 2015, SoPh, 290, 2479
Hatanaka, T. 1956, PASJ, 8, 73
Isbell, D. 1960, IRE Transactions on Antennas and Propgation, 8, 260
Jamil, A., Yusoff, M. Z., Yahya, N., & Zakariya, M. A. 2011, in IEEE Conf. on Open Systems (New York: IEEE), 290
Jin, S.-Z., Zhao, R.-Y., & Fu, Q.-Y. 1986, SoPh, 104, 391
Jingjing, H., Zhiwen, X., Yang, Y., Jianguo, H., & Peiguo, L. 2008, in Int. Conf. on Microwave and mmwave Technology (New York: IEEE), 1849
Jiricka, K., Karlicky, M., Kepka, O., & Tlamicha, A. 1993, SoPh, 147, 203
Jones, K. E., & Mayes, P. E. 1969, ITAP, 1, 2
Karim, M. N. A., Rahim, M. K. A., Majid, H. A., et al. 2010, PIRE, 100, 201
Kaverin, N. S., Kobrin, M. M., Korshunov, A. I., & Shushunov, V. V. 1979, SoPh, 63, 379
Keen, K. M. 1974, ITAP, 22, 489
Kishore, P., Kathiravan, C., Ramesh, R., et al. 2014, SoPh, 289, 3995
Kishore, P., Ramesh, R., Kathiravan, C., & Rajalingam, M. 2015, SoPh, 290, 2409
Kontogeorgos, A., Tsitsipis, P., Caroubalos, C., et al. 2006, ExA, 21, 41
Kraus, J. D. 1950, Antennas (Singapore: McGraw-Hill)
Kumari, A., Ramesh, R., Kathiravan, C., et al. 2019, ApJ, 881, 24
Kyei, A., & Jung, Y.-B. 2018, ITAP, 66, 6762

Kyei, A., Sim, D.-U., & Jung, Y.-B. 2017, IET Microw. Antennas Propag., 11, 711

Lanzerotti, L. J. 2004, Solar and Space Weather Radiophysics (Astrophysics and Space Science Library) Vol. 314(Berlin: Springer), 1

Lee, K. F., Luk, K. M., & Mak, K. M. 2010, Microw. Opt. Technol. Lett., 52, 1498

Mann, G., Auras, B., Voigt, W., & Paschke, J. 1992, in ESA SP-348, Proc. 1st SOHO Workshop (Noordwijk: ESA), 129

McLean, D. J. 1985, Solar Radiophysics (Cambridge: Cambridge Univ. Press)

Moallemizadeh, A., Hassani, H. R., & Mohamed Ali nezhad, S. 2012, in 6th European Conf. IEEE Antennas and Propagation (EUCAP) (New York: IEEE)

Morosan, D. E., Rasanen, J. E., Kumari, A., et al. 2022, SoPh, 297, 47

Mosier, S. R., & Fainberg, J. 1975, SoPh, 40, 501

Pantoja, R., Sapienza, A., & Filho, F. M. 1987, ITAP, 35, 1176

Peixeiro, C. 1988, IEEEP, 135, 98

Perrenoud, M. R. 1982, SoPh, 81, 197

Pitzer, T. L., Fellows, J. A., Lamont, G. B., & Terzuoli, A. J. 2006, in IEEE Int. Conf. on Evolutionary Computation (New York: IEEE), 3189

Pivnenko, S. 2006, in First European Conf. on Antennas and Propagation (New York: IEEE)

Prestage, N. P. 1995, JATP, 57, 1815

Puente-Baliadra, C. P., & Pous, R. 1996, ITAP, 44, 730

Puricer, P., Kovar, P., & Barta, M. 2019, Electronics, 8, 861

Qiu, J., Lin, S., Yang, C., & You, Q. 2005, in 5th IEEE Int. Conference MEMIA'05 (New York: IEEE), 6150

Rahman, N. A., & Jamlos, M. F. 2016, in Proc. of the Int. Conf. on Computer and Communication Engineering (New York: IEEE), 53

Ramesh, R. 2011, in ASI Conf. Ser. 2,, ed. A. R. Choudhuri & D. Banerjee (Hyderabad: ASI), 55

Ramesh, R., & Kathiravan, C. 2022, ApJ, 940, 80

Ramesh, R., Kathiravan, C., Indajit, V., et al. 2010, ApJL, 719, 41

Ramesh, R., Mugundhan, V., & Prabhu, K. 2020, ApJL, 889, 25

Ramesh, R., Subramanian, K. R., Sundararajan, M. S., & Sastry, Ch. V. 1998, SoPh, 181, 439

Rashed, J., & Tai, C.-T. 1991, ITAP, 39, 1428

Reid, H. A. S., & Ratcliffe, H. 2014, RAA, 14, 773

Ripin, N., Saidy, W. M. A. W., Sulaiman, A. A., et al. 2013, in IEEE Student Conference on Research and Devlopment (New York: IEEE), 365

Sasikumar raja, K., Kathiravan, C., Ramesh, R., Rajalingam, M., & Indrajit, V. Barve 2013, ApJS, 207, 2

Sawant, H. S., Subramanian, K. R., Faria, C., et al. 2001, SoPh, 200, 167

Schwenn, R. 2006, LRSP, 3, 2

Simpson, T. L. 1971, ITAP, 19, 186

Strycek, M., & Hertl, I. 2007, in Proc. on 17th Int. Conf. on Radioelektronica (New York: IEEE)

Stutzman, W. L., & Thiele, G. A. 1981, Antenna Theory and Design (New York: Wiley)

Sun, Q., Wang, J., Cui, J., et al. 2014, in 3rd Asia-Pacific Conference on Antennas and Propagation (New York: IEEE), 593

The ARRL Antenna Book 1991, The American Radio Relay League (Newington, CT: ARRL)

Thompson, A. R. 1961, ApJ, 133, 643

Tingay, S. J., Goeke, R., Bowman, J. D., et al. 2013, PASA, 30, 7

Van Haarlem, M. P., Wise, M. W., Gunst, A. W., et al. 2013, A&A, 556, A2

Van Nieuwkoop, J. 1971, PhD thesis, Univ. Utrecht

Wakabayashi, R., Shimada, K., Kawakami, H., & Sato, G. 1999, ITElC, 41, 93

Wild, J. P., & McCready, L. L. 1950, AuSRA, 3, 387

Wild, J. P., Murray, J. D., & Rowe, W. C. 1954, AuJPh, 7, 439

Wu, P. R. 1969, ITAP, 17, 428

Zhai, G., Wang, X., Xie, R., et al. 2019, ITAP, 67, 6193

Zucca, A., Carley, E. P., McCauley, J., et al. 2012, SoPh, 280, 591